ULTRA-LOW NOISE FIBER LASER SYSTEMS AND THEIR APPLICATIONS

A DISSERTATION SUBMITTED TO
THE DEPARTMENT OF PHYSICS
AND THE GRADUATE SCHOOL OF ENGINEERING AND SCIENCE
OF BILKENT UNIVERSITY
IN PARTIAL FULFILLMENT OF THE REQUIREMENTS
FOR THE DEGREE OF
DOCTOR OF PHILOSOPHY

By
İbrahim Levent Budunoğlu
January, 2014

I certify that I have read this thesis and that in my opinion it is fully adequate, in scope and in quality, as a dissertation for the degree of Doctor of Philosophy.

Assoc. Prof. Dr. Fatih Ömer İlday(Advisor)

I certify that I have read this thesis and that in my opinion it is fully adequate, in scope and in quality, as a dissertation for the degree of Doctor of Philosophy.

Assoc. Prof. Dr. Hakan Altan

I certify that I have read this thesis and that in my opinion it is fully adequate, in scope and in quality, as a dissertation for the degree of Doctor of Philosophy.

Assoc. Prof. Dr. M. Özgür Oktel

I certify that I have read this thesis and that in my opinion it is fully adequate, in scope and in quality, as a dissertation for the degree of Doctor of Philosophy.

Assist. Prof. Dr. Bülend Ortaç

I certify that I have read this thesis and that in my opinion it is fully adequate, in scope and in quality, as a dissertation for the degree of Doctor of Philosophy.

Assist. Prof. Dr. Aykutlu Dâna

Approved for the Graduate School of Engineering and Science:

Prof. Dr. Levent Onural
Director of the Graduate School

ABSTRACT

ULTRA-LOW NOISE FIBER LASER SYSTEMS AND THEIR APPLICATIONS

İbrahim Levent Budunoğlu
PhDin Physics
Supervisor: Assoc. Prof. Dr. Fatih Ömer İlday
January, 2014

Fiber laser systems are intensely studied for and already utilized in a wide range of scientific, biomedical and industrial applications. Scientifically, fiber lasers are widely used for spectroscopy, laser-matter interactions, nonlinear and quantum optics experiments, among others. The industrial applications range from the well-established, such as laser-material processing, laser marking, and various forms of optical sensing to niche or upcoming applications such as high-speed circuit testing, inspection of packaged foods, additive manufacturing. In all applications outside the research laboratory, long-term stability of the lasers operation is of paramount importance. Fiber lasers are clearly advantageous in this respect, as the optical fibers provide isolated paths for light propagation, minimizing the impact of environmental effects, and generally render the laser system nearly or completely free from mechanical misalignment. In addition to long-term stability of the laser operation, short-term (typically less than 1 second) stability, or fluctuations of the laser output is of crucial importance as in many situations, it effectively determines the signal-to-noise ratio, sets the resolution or otherwise limits the quality of the measurement. Fluctuations or noise impact both the intensity and phase of the laser output.

As part of this thesis, first, the intensity noise of mode-locked fiber lasers is characterized systematically for the major mode-locking regimes over a wide range of parameters. It is found that equally low-noise performance can be obtained in all regimes. Losses in the cavity influence noise strongly without a clear trace in the pulse characteristics. Noise level is found to be virtually independent of pulse energy below a threshold for the onset of nonlinearly induced instabilities. Instabilities that occur at high pulse energies are characterized. It is found that continuous-wave peak formation and multiple pulsing influence noise performance

moderately. However, at high pulse energies, an abrupt increase of the intensity noise is encountered, corresponding to up to 2 orders of magnitude increase in noise. These results effectively constitute guidelines for minimization of the laser noise in mode-locked fiber lasers. For the high-power laser systems that utilize external amplification in fiber amplifiers, the added noise due to amplification is usually predominantly determined by the pump source, assuming that the amplifier design is correctly made and amplified spontaneous emission (ASE) is minimized. Many high-power amplifiers utilized multi-mode pump diodes, which have much higher noise levels. A high-power fiber laser system where the amplifiers are seeded by low intensity noise pulses is analyzed in detail. When operating at its maximum power level (10 W), the amplified output exhibits an integrated (from 3 Hz to 250 kHz) intensity noise of 0.2%, whereas the seed signals intensity noise is less than 0.03%. The origins of the added noise is analyzed systematically using modulation transfer functions to ascertain contributions of the pump source. The transfer of the noise in the seed signal is also analyzed, as well as contributions of ASE, which can be significant. Prediction of intensity noise by modulation transfer functions supplies a lower limit for the intensity noise of fiber lasers and amplifiers.

The second part of the thesis applies the know-how on low-noise fiber lasers that was developed in the first part to a scientific problem. As part of a collaboration with researchers from Ruhr-University at Bochum, Germany, we have developed a custom, low-noise laser system for spectroscopy of micro-plasma discharges. Absorption spectroscopy is a commonly used technique to determine the presence of a particular substance or to quantify the amount of substance present in the plasma discharge. However, the absorbance is usually small, at the level of one part in a thousand or less. Therefore, low-noise laser signals are required to detect such low differences. We developed a low-noise fiber laser system for the absorption spectroscopy studies of reactive species in a micro-plasma discharge. The laser setup also produces high-energy picosecond pulses, which are powerful enough to trigger the plasma ignition and transition into other transient states of plasma. Since both pulses are generated from the same mode-locked oscillator, they have excellent mutual synchronization. We demonstrate the possibility for pump-probe experiments by initiating breakdown on a picosecond time scale (pump) with a high-power beam and measuring the broadband absorption with the simultaneously provided supercontinuum (probe).

The third part of this thesis the laser-noise know-how to address a technological problem, namely the development custom, low-noise fiber lasers for LADAR applications. Two different fiber laser systems are constructed as transmitter sources of direct detection and coherent detection LADAR systems and tested for realistic scenarios. Both LADAR systems succeeded to detect 1 cm-diameter wire from a distance of 1 km in a measurement time shorter than 100 s, which is comparable to the best performing commercial LADAR systems.

Keywords: Fiber laser, Fiber amplifier, Relative intensity noise, Modulation transfer function, Absorption spectroscopy, Ladar, Direct detection, Coherent detection.

ÖZET

ULTRA-DÜŞÜK GÜRÜLTÜLÜ FİBER LAZER SİSTEMLERİ VE UYGULAMALARI

İbrahim Levent Budunoğlu
Fizik, Doktora
Tez Yöneticisi: Assist. Prof. Dr. Fatih Ömer İlday
Ocak, 2014

Günümüzde fiber lazer sistemleri, bilimsel, biomedikal ve endüstriyel uygulamalarda yoğun şekilde kullanılmaktadır. Spektroskopi, lazer-malzeme etkileşimi, doğrusal olmayan ve kuvantum optik deneyleri gibi pekçok bilimsel alanda yer bulurken, aynı zamanda, malzeme işleme, lazer markalama ve yüksek hızlı devre testi gibi pekçok endüstriyel uygulamada da yer edinmiştir. Tüm bu uygulamalar için uzun-vade kararlılığı en önemli gerekliliklerin arasında gelir. Bu bakımdan fiber lazerler büyük avantaja sahiptir. Optik fiberler, ışığın izole edilmiş bir yoldan geçmesini sağlayarak hem çevrenin etkisini en aza indirir, hem de mekanik sebepler sonucu ışığın sapmasını engeller. Uzun-vade kararlılığın yanısıra kısa-vade (1 saniye ve altı) kararlılığı ve lazer çıkışındaki dalgalanmalar da uygulamalar için hayati önem taşır. Kısa-vade kararlılığı, ölçümlerin sinyal-gürültü oranını, ölçüm ve işlem çözünürlüğünü belirleyen başlıca parametredir.

Öncelikle, kip-kilitli lazerlerin şiddet gürültüsü tüm bilindik kip-kilitleme rejimleri için, geniş bir parametre aralığında, sistematik olarak karakterize edilmiştir. Şiddet gürültüsünün kip-kilitleme rejimine bağlı olmadığı anlaşılmıştır. Kovuk kayıpları atım karakteristiklerinde belirgin bir iz bırakmazken, gürültü performansını şiddetli bir şekilde etkilemektedir. Sürekli-dalga veya çoklu atım oluşumu, gürültü performansını bir dereceye kadar etkilemektedir. Fakat daha yüksek enerji seviyelerinde, gürültü seviyesinin 100 kat mertebesinde artışına sebep olan gürültü patlaması gözlemlenmiştir. Bu sonuçlar kip-kilitli fiber lazerlerde şiddet gürültüsünü azaltma yöntemleri üzerine önemli değerlendirmeler sunmaktadır. Yüksek güçlü lazer sistemlerinde nihai gürültü seviyesini, yükseltme sırasında pompa diyodundan aktarılan gürültü belirler. Ultra-düşük gürültülü fiber lazer tarafından beslenen yüksek güçlü bir fiber lazer sistemi, gürültü açısından incelenmiştir. Sistem en yüksek güç kapasitesinde (10 W)

çalıştığı sırada %0.2'den daha düşük gürültü (3 Hz'den 250 kHz'e entegre edilmiş) seviyesinde atımlar üretmektedir. Ek olarak, gürültü kaynakları, modülasyon aktarım fonksiyonu yaklaşımıyla sistematik olarak karakterize edilmiştir. Bu fonksiyonlar kullanılarak nihai atımların gürültü seviyelerinin tahmin edilebileceği gösterilmiştir.

Düşük gürültülü fiber lazerler konusunda elde edilmiş bilgi birikimi, tezin ikinci bölümünde bilimsel bir problemin çözümünde kullanılmıştır. Ruhr üniversitesi araştırmacıları ile sürdürülen ortak çalışmanın bir ürünü olarak, mikro-plazma deşarjı spektroskopisinde kullanılmak üzere, düşük-gürültülü fiber lazer sistemi geliştirilmiştir. Soğrulma spektroskopisi, bir maddenin varlığını ve miktarını tespit etmek için plazma deşarjı üzerinde kullanılan en temel yöntemlerden birisidir. Lazer ışığının soğrulması çoğu zaman çok düşük miktarlarda olduğundan (binde bir veya daha az), bunu algılayabilmek için ultra-düşük gürültülü sistemler gerekmektedir. Bu bağlamda mikro-plazma üzerinde soğrulma spektrosposi çalışmalarında kullanılmak üzere geniş spektrumlu düşük gürültülü atımlar üreten bir fiber lazer düzeneği geliştirilmiştir. Düzenek aynı zamanda plazma oluşumunu başlatabilecek enerji seviyesinde atımlar da üretebilmektedir. Her iki türdeki atımlar aynı fiber lazerin beslemesiyle üretildiğinden, aralarındaki zamanlama çok yüksek seviyededir. Bu sistemle birlikte, mikro-plazma jetlerinde pompalama-ölçme (pump-probe) deneyleri yapabilme imkanı doğmuştur.

Tezin üçüncü bölümünde lazer gürültüsü konusundaki bilgi birikimi, düşük gürültülü LADAR uygulamalarında kullanılacak fiber lazer geliştirmesi için kullanılmıştır. Evre-uyumlu ve doğrudan algılama ladar sistemleri için kullanılmak üzere iki adet fiber lazer sistemi geliştirilmiş ve gerçekçi senaryolar ile denenmiştir. Her iki sistem de 1 km mesafeden 1 cm çapındaki enerji nakil hattını 100 μsden daha kısa ölçüm süresinde algılayabilme yeteneğini göstermiştir. Bu performans satılan en üstün ticari ürünler ile karşılaştırılabilir düzeydedir.

Anahtar sözcükler: Fiber lazer, Fiber yükseltici, Görece şiddet gürültüsü, Modülasyon aktarım fonksiyonu, Soğrulma spektroskopisi, Ladar, Doğrudan algılama, Evre-uyumlu algılama.

Acknowledgement

I would like to express my deepest gratitude to my supervisor F. Ömer İlday for his invaluable guidance, support and encouragement. His experiences and guidance enabled me to develop a scientific understanding of the subject. Furthermore, he helped me to learn how to become an individual scientist and stubbornly overcome the problems, which I believe will be the best experience for the rest of my life.

I would like to thank all the former and present group members of UFOLAB for being helpful and friendly to me.

I would especially like to thank Mutlu Erdoğan and Kıvanç Özgören for the fruitful scientific discussions.

I would especially like to thank Kutan Gürel and Coşkun Ülgüdür for their collaborations till the early mornings.

I would also like to thank Electro-Optic System Engineering group members of Meteksan Savunma. I am thankfull to Kaan Akar for his fruitfull discussions and Ebru Bayrı for her collaboration.

The financial support from TÜBITAK and Bilkent University are also gratefully acknowledged.

Last but not the least; I would like to thank my parents Hatice and Mustafa Budunoğlu in addition to my sister Emel Ögütçü for their support during my education.

Finally, I wish to give my special thanks to my lovely wife Hülya, my dearest daughter Ece, and new born baby boy Ege for their patience during this hard and tiring period, their patience and endless love.

To Hülya, Ece and Ege

Contents

List of Figures

List of Tables

Chapter 1

Introduction

Light has attracted the curiosity of mankind since the dawn of our race. This interest in light penetrated many fields of human practice, including philosophy, art, science, technology and religion. In ancient Greek philosophy, Aristotle wrote on the properties of *camera obscura*. Art has used light both as a symbol and a tool for expressing aspects of reality. Throughout ages, absence of light has long been associated with depression, decay or outright evil. Reciting a recent, popular example, in the blockbuster movie, Star Wars, the Dark Side represents evil. In the art of photography, the same scene can express quite different emotions under different lighting conditions. In Christianity, divinity is represented by an aura of light and in Islam, the divine purity is expressed by the word "nur" (*i.e.*, light). The interest in light, combined with a mystic sense of wonder about its nature, has led to the development of the science of light (*i.e.*, optics), taking modern form starting with Pierre de Fermat, continuing Isaac Newton, up to the modern understanding offered by the electromagnetic theory of James Clerk Maxwell, culminating in our contemporary understanding based on the quantum theory of light. In parallel to the scientific development of the science of light, the impact of optical technologies on the daily life of the layman has been tremendous, ranging from the development of the corrective lenses to the fiber-optic technology that forms the backbone of the Internet, not to mention the pivotal role of the microscope in the development of modern medicine. Today's world is teeming with technologies based on optics.

Light is an object of physical inquiry, examined to uncover its nature. It is an entry point into understanding the universe because photon is one of the fundamental particles, the mediator of one of the four fundamental forces, the electromagnetic force, which underlies all chemical and biological processes virtually single-handedly. At the same time, light is the main source of our knowledge about the universe (*e.g.*, consider astronomy, which would have been possible with the telescope, and optical imaging techniques, which have transformed the medical sciences and biology). The author believes that the simplicity, the beauty and the explanatory power of optics may show that properties of light might provide a good analogy for the whole universe. Even the most complex physical structures (*e.g.*, organisms) are governed by electromagnetic forces. These complex structures emerge out of simple and universal regularities in which electromagnetism is an essential part.

The main motivation of the author for pursuing a research career in optics is his belief that simple optical solutions can be found for diverse problems. For instance, laser beams can be used to probe neuronal activity, discover planets orbits star eons away, or map out the evolution of molecular reactions, or even the dynamics of individual electrons. The driving motto of the author is "to find optical solutions".

Fiber lasers provide a very convenient platform for producing high-quality and task-specific laser signals, which can be applied to a wide variety of scientific and technological problems. The ability of laser beams to be propagated through optical fibers makes it possible to deliver light through complicated paths (*e.g.*, in vivo delivery of light to particular body part) or to otherwise largely inaccessible locations (*e.g.*, deep underground or depths of the oceans). Furthermore, the modular structure of fiber lasers, utilizing master-oscillator, power-amplifier (MOPA) architectures, makes them adaptable for various applications. Furthermore, fiber lasers are compact in size and robust in their operation under harsh conditions. Moreover, ultrafast lasers have rich dynamics, which would attract scientific interest.

Probing information by using laser requires high-quality beams and stable laser operation. One of the main indicators of the stability of lasers is the relative intensity noise (RIN). In this theses, we report the characterization of the RIN of fiber lasers and amplifiers for various parameters and develop a technique to predict the RIN of fiber lasers and amplifiers. We also mention some practical approaches to produce low noise fiber laser systems. The following chapters describe the application of our low-noise laser know-how first to a scientific and then to a technological problem. The concluding chapter summarizes the main results of this thesis and provides an outlook.

Chapter 2

Fiber Lasers and Amplifiers

2.1 Light Propagation in Fibers

An optical waveguide is a structure that can guide a light beam from one point to another and the most commonly used waveguide is the step-index optical fiber (Figure 2.1). A step-index fiber has a cylindrical shape and consists of a central dielectric core, a cladding region, also a dielectric material of a slightly lower refractive index.

$$\begin{aligned} n(r) &= n_1, r < a \\ n(r) &= n_2, r > a, \end{aligned} \tag{2.1}$$

where a is the core radius. If the angle of incidence ϕ of a ray entering the fiber as shown in Figure 2.1 is greater than the critical angle

$$\phi_c = \sin^{-1}\left(\frac{n_2}{n_1}\right), \tag{2.2}$$

total internal reflection guides the light through the fiber. This phenomenon was firstly demonstrated by John Tyndall in 1854 where he showed that light propagates along the curved path of water. Although uncladded fibers were fabricated in the 1920s [1], fiber optics really developed in the 1950s with the works of Van Heel in Holland [2] and Hopkins and Kapany [3] in the United

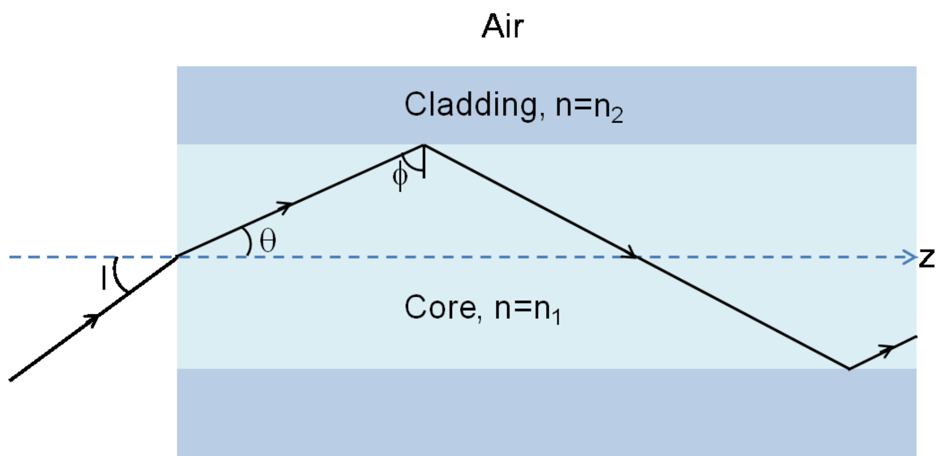

Figure 2.1: Step-index fiber.

Kingdom. They started to use a cladding layer, which led to improvements in fiber characteristics.

There are two main parameters that characterize an optical fiber: numerical aperture and the V parameter. Numerical aperture defines the angle of acceptance for a fiber. When a cone light is incident on one end of the fiber, it will be guided if the semi-angle of the cone is less than i_{m} where

$$\sin i_{\mathrm{m}} = \left(n_1^2 - n_2^2\right)^{\frac{1}{2}}. \tag{2.3}$$

This angle is a measure of the light-gathering power of the fiber and, by using it, one defines the numerical aperture of the fiber by the following equation

$$NA = \left(n_1^2 - n_2^2\right)^{\frac{1}{2}}. \tag{2.4}$$

The V parameter determines the number of modes supported by the cylindrical geometry of the fiber and can be driven from the wave equation. In cylindrical coordinates the wave equation for the electric field, E, in the Fourier domain can be written as:

$$\frac{\partial^2 \tilde{E}}{\partial \rho^2} + \frac{1}{\rho}\frac{\partial \tilde{E}}{\partial \rho} + \frac{1}{\rho^2}\frac{\partial^2 \tilde{E}}{\partial \phi^2} + \frac{\partial^2 \tilde{E}}{\partial z^2} + n^2 k_0^2 \tilde{E} = 0, \tag{2.5}$$

where $k_0 = \omega/c = 2\pi/\lambda$. The same equation can be written for the magnetic field, H. Due to the Maxwell's equations it is enough to solve the equation at only z-direction. Let us use the separation of variables method and write

$$\tilde{E}_{\mathrm{z}}(r,\omega) = A(\omega)\, F(\rho)\, exp(im\phi)\, exp(i\beta z)\,, \tag{2.6}$$

where A is normalization constant, β is propagation constant, and m is an integer,

$$\frac{d^2F}{d\rho^2} + \frac{1}{\rho}\frac{dF}{d\rho} + \left(n^2k_0^2 - \beta^2 - \frac{m^2}{\rho^2}\right)F = 0. \tag{2.7}$$

Here, the refractive index n is equal to n_1 for core and n_2 for cladding. The only physically meaningful solution of this equation is the Bessel function. Thus, inside the core,

$$F(\rho) = J_{\mathrm{m}}(\kappa\rho), \qquad\qquad \rho \le a, \tag{2.8}$$

and in the cladding region

$$F(\rho) = K_{\mathrm{m}}(\gamma\rho), \qquad\qquad \rho \ge a, \tag{2.9}$$

where

$$\kappa = \left(n_1^2k_0^2 - \beta^2\right)^{\frac{1}{2}} \tag{2.10}$$

$$\gamma = \left(\beta^2 - n_2^2k_0^2\right)^{\frac{1}{2}} \tag{2.11}$$

$$\kappa^2 + \gamma^2 = \left(n_1^2 - n_2^2\right)k_0^2. \tag{2.12}$$

By solving the equation also for H and applying the boundary conditions, where the tangential components of E and H are to be continuous across the core-cladding interface, one can write the eigenvalue equation below:

$$\left[\frac{J'_{\mathrm{m}}(\kappa a)}{\kappa J_{\mathrm{m}}(\kappa a)} + \frac{\kappa'_{\mathrm{m}}(\gamma a)}{\gamma\kappa_{\mathrm{m}}(\gamma a)}\right]\left[\frac{J'_{\mathrm{m}}(\kappa a)}{\kappa J_{\mathrm{m}}(\kappa a)} + \frac{n_2^2}{n_1^2}\frac{\kappa'_{\mathrm{m}}(\gamma a)}{\gamma\kappa_{\mathrm{m}}(\gamma a)}\right] = \left(\frac{m\beta k_0\left(n_1^2 - n_2^2\right)}{an_1\kappa^2\gamma^2}\right)^2, \tag{2.13}$$

where the prime denotes differentiation. Each eigenvalue of β_{mn} corresponds to one specific mode supported by the fiber. The value of κ when $\gamma = 0$ for a given mode defines the cut-off frequency from Eq. 2.12 and the V parameter is defined as

$$V = \kappa_c a = k_0 a (n_1^2 - n_2^2)^{1/2}. \tag{2.14}$$

For single mode operation, V parameter should be smaller than 2.405 and higher modes are beyond cutoff.

2.2 Pulse Propagation in Fibers

In the previous section, the linear wave equation Eq. 2.5 has been used by assuming that the response of the material is a linear function of light intensity and ignoring dependance of the index of refraction on wavelength, *i.e.*, dispersion. However, while dealing with the pulses propagating inside a fiber, one should consider the response of the material. Ultrashort pulses have large spectral bandwidths and high peak powers, thus some effects, which may be negligible for continuous-wave operation becomes important for pulse operation. Let us rewrite the wave equation:

$$\vec{\nabla}^2 \vec{E} - \frac{1}{c^2}\frac{\partial^2 \vec{E}}{\partial t^2} = \mu_0 \frac{\partial^2 \vec{P}}{\partial t^2} \tag{2.15}$$

Here, the response of the material is given in closed form as $\vec{P}$ polarization vector. This equation can be driven by using the Maxwell equations. Now we will begin to work on this equation by defining what $\vec{P}$ is. Polarization is the reactance of the material to the applied electric field on it. One can consider a spring driven by time-dependent force as analogy. In this analogy, polarization represents the displacement (response of the spring) and E-field represents the time-dependent force. Since the higher-order terms have much less coefficients, it can be expanded as:

$$\vec{P} = \epsilon_0(\chi^{(1)}\vec{E} + \chi^{(2)}\vec{E}^2 + \chi^{(3)}\vec{E}^3 + \ldots) = \vec{P}_{\text{linear}} + \vec{P}_{\text{nonlin}} \tag{2.16}$$

At higher amplitudes, higher-order terms should be considered. Another important point is that, the response function $\vec{P}$ also depends on the frequency of the E-field. All materials have some characteristic resonance frequencies at which the medium absorbs the electromagnetic radiation through oscillations of bound electrons. Far from the resonance frequencies, the refractive index can be written as

$$n^2(\omega) = 1 + \sum_{j=1}^{m} \frac{B_{\mathrm{j}}\omega_{\mathrm{j}}^2}{\omega_{\mathrm{j}}^2 - \omega^2} \tag{2.17}$$

using Sellmeir equation [4]. Thus, if we reflect frequency dependency of the material to the first term of the polarization, the linear equation can be written as:

$$\overrightarrow{P}_{\text{linear}}(\omega) = \epsilon_0 \chi^{(1)}(\omega) \overrightarrow{E}(\omega), \tag{2.18}$$

and the wave equation can be written in the Fourier domain as follows,

$$(\overrightarrow{\nabla}^2 + \frac{\omega^2}{c^2}(1 + \chi^{(1)}))\overrightarrow{E}(\omega) = -\mu_0 \omega^2 \overrightarrow{P}_{\text{nonlin}}. \tag{2.19}$$

As seen above,the wave equation covers both the frequency dependence (dispersion) and the nonlinear response (nonlinearity). The solution of this equation will give more precise function of light including high bandwidth and high energy signals in the fiber. The electric field has a time structure that has a slow and a fast varying component, where the fast time scale corresponds to the optical cycle and the slow time scale corresponds to the width of the wavepackets. Thus we can separate them in order to simplify:

$$\overrightarrow{E}(\overrightarrow{r}, t) = \overrightarrow{A}(\overrightarrow{r}, t) exp(ik_0 z - i\omega_0 t) + c.c. \tag{2.20}$$

$$\overrightarrow{P}(\overrightarrow{r}, t) = \overrightarrow{P}'(\overrightarrow{r}, t) exp(ik_0 z - i\omega_0 t) + c.c. \tag{2.21}$$

In the time domain, we are writing the fields as an envelope times a field that oscillates rapidly at the optical frequency ω_0. We choose ω_0 to be the center frequency of the optical spectrum of the pulse. In the frequency domain, this is equivalent to

$$\overrightarrow{E}(\overrightarrow{r}, \omega) = \int_{-\infty}^{+\infty} \overrightarrow{A}(\overrightarrow{r}, t) exp(ik_0 z - i\omega_0 t) exp(i\omega t) \tag{2.22}$$

$$= \overrightarrow{A}(\overrightarrow{r}, \omega - \omega_0) exp(ik_0 z). \tag{2.23}$$

If the equations 2.15, and 2.16 are used and it is assumed that the field is polarized in a fixed direction in the plane perpendicular to the direction of propagation, wave equation can be rewritten as follows:

$$(\frac{\partial^2}{\partial z^2}+\frac{\partial^2}{\partial x^2}+\frac{\partial^2}{\partial y^2}+2ik_0\frac{\partial}{\partial z}-k_0^2)A(x,y,t)+k^2(\omega)A(x,y,t) = -\mu_0\omega^2 P'_{\text{nonlin.}}, \quad (2.24)$$

where, $\chi^{(1)}(\omega) = \frac{c^2}{\omega^2}k^2(\omega) - 1$. On the left side of the equation, the first term represents the spatial diffraction and second term represents the dispersion. The right side of the equation includes the nonlinear correction term. Here k number includes the frequency dependent response of the material and by using the Taylor expansion around ω_0, it can be written as:

$$k(\omega) = k(\omega_0) + k'(\omega_0)(\omega-\omega_0) + \frac{1}{2!}k''(\omega_0)(\omega-\omega_0)^2 + \frac{1}{3!}k'''(\omega_0)(\omega-\omega_0)^3 + \cdots, \quad (2.25)$$

where prime denotes derivation with respect to ω. These terms represent the phase velocity, group velocity and group velocity dispersion, respectively and higher-order terms represent the higher-order dispersion relations. Now let us write the wave equation again around central frequency ($\omega' = \omega - \omega_0$) in time domain:

$$\begin{aligned}(\frac{\partial^2}{\partial z^2}+\frac{\partial^2}{\partial x^2}+\frac{\partial^2}{\partial y^2}+2ik_0\frac{\partial}{\partial z}-k_0^2)A(x,y,t)+\\ (k_0+ik_1\frac{\partial}{\partial t}-\frac{1}{2}k_2\frac{\partial^2}{\partial t^2}+\ldots)A(x,y,t)=\\ -\mu_0(\omega_0+i\frac{\partial}{\partial t})^2 P'_{\text{nonlin.}}\end{aligned} \quad (2.26)$$

We will transform all the variables in the reference frame of the wavepacket; $(z,t) \rightarrow (z, \tau = t - z/v_g)$. By applying the chain rule,

$$\frac{\partial}{\partial z} = \frac{\partial}{\partial z} + \frac{\partial}{\partial \tau}\frac{\partial \tau}{\partial z} = \frac{\partial}{\partial z} - k_1\frac{\partial}{\partial \tau} \quad (2.27)$$

$$\frac{\partial}{\partial t} = \frac{\partial}{\partial z}\frac{\partial z}{\partial t} + \frac{\partial}{\partial \tau}\frac{\partial \tau}{\partial t} = \frac{\partial}{\partial \tau} \quad (2.28)$$

we can write the master equation as

$$\begin{aligned}(\frac{\partial^2}{\partial z^2}+\frac{\partial^2}{\partial x^2}+\frac{\partial^2}{\partial y^2})A'(x,y,\tau)+i2k_0(1-\frac{k_1}{k_0}\frac{\partial}{\partial \tau})\frac{\partial}{\partial z}A'(x,y,\tau)+\\ (2k_0(1+i\frac{k_1}{k_0}\frac{\partial}{\partial \tau})D+D^2)A'(x,y,\tau) = -\mu_0\omega_0^2(1+i\frac{1}{\omega_0}\frac{\partial}{\partial \tau})^2 P'_{\text{nonlin.}}\end{aligned} \quad (2.29)$$

We will make the so-called slowly varying envelope approximation (SVEA) both in time and space domains and ignore the dispersion terms higher than the second order. The SVEA in time domain is applicable when the pulse is longer than a few optical cycles of carrier signal, then it can be written that $k_1/k_0 = c/(n_0\omega_0 v_g) = \frac{1}{\omega}\frac{v_P}{v_g} \sim \frac{1}{\omega} \quad \Rightarrow \quad \frac{k_1}{k_0}\frac{\partial}{\partial\tau} \sim \frac{T_{\text{carier}}}{T_{\text{pulse}}} \ll 1$. The SVEA in space domain is valid if the beam size is bigger than a few wavelengths of the carrier and similarly it can be written that $\frac{\partial^2 A'}{\partial z^2} \ll k_0\frac{\partial A'}{\partial z}$. Then the wave equation in time domain can be simplified as below :

$$\frac{\partial A'}{\partial z} - i\frac{1}{2k_0}(\frac{\partial^2}{\partial x^2} + \frac{\partial^2}{\partial y^2})A' + i\frac{1}{2}k_2\frac{\partial^2 A'}{\partial \tau^2} = i\frac{\mu_0\omega_0^2}{2k_0}P'_{\text{nonlin.}} \tag{2.30}$$

Now we begin to consider the nonlinear term on the right side of the equation $P_{\text{nonlin}} = \epsilon_0\left(\chi^{(2)}\overrightarrow{E}^2 + \chi^{(3)}\overrightarrow{E}^3 + \cdots\right)$. We will consider only the odd terms since even term nonlinearities are zero for centrosymmetric materials. Furthermore, we can ignore the terms higher than third order, thus we will only consider $\chi^{(3)}$. Hence we can rewrite the wave equation as

$$\frac{\partial a}{\partial z} - i\frac{1}{2k_0}(\frac{\partial^2}{\partial x^2} + \frac{\partial^2}{\partial y^2})a + i\frac{1}{2}k_2\frac{\partial^2 a}{\partial \tau^2} = i\frac{2\pi n_2}{\lambda_0}|a|^2 a, \tag{2.31}$$

where $|a|^2$ is the optical intensity and $n_2 \equiv \frac{3}{8n_0}\chi^{(3)}$ is the nonlinear refraction index where $n = n_0 + n_2|a|^2$. This equation is called nonlinear Schroedinger equation.

2.3 Gain in Fiber Amplifiers

Gain through an optical fiber has the dynamics similar to other gain media apart from geometrical differences. Furthermore, gain dynamics is too slow to distinguish individual pulses, thus gain equations for continuous-wave operation are also valid for ultrafast pulses. Only the pulses which are comparable or longer than the upper-state lifetime of the gain medium should be considered in more detail but this is beyond the scope of this thesis.

To create gain medium inside optical fibers, suitable types of atoms are doped into the core of the fibers. The gain can have a three-level or four-level scheme

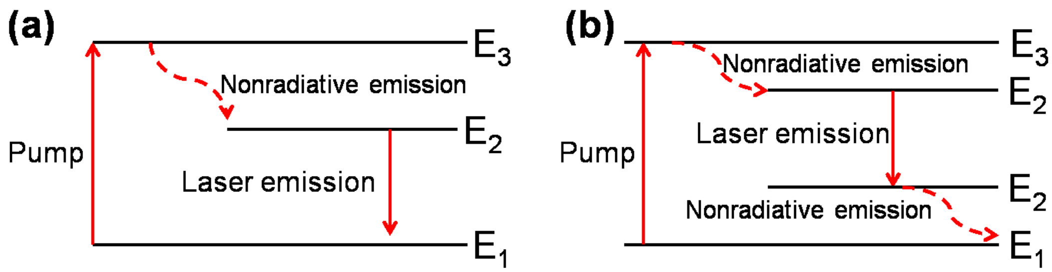

Figure 2.2: Energy levels of (a) three level and (b) four level systems.

according to the dopants energy levels as shown in Figure 2.2. Let us consider a three-level system. The rate equations can be written as

$$\frac{\partial n_3}{\partial t} = -\frac{1}{\tau_{32}} n_3 - \frac{1}{\tau_{31}} n_3 + \frac{\sigma_{13} I_p}{h\nu_p} n_1 - \frac{\sigma_{31} I_p}{h\nu_p} n_3 \tag{2.32}$$

$$\frac{\partial n_2}{\partial t} = -\frac{1}{\tau_{21}} n_2 + \frac{1}{\tau_{32}} n_3 + \frac{\sigma_{12} I_s}{h\nu_s} n_1 - \frac{\sigma_{21} I_s}{h\nu_s} n_2 \tag{2.33}$$

$$\frac{\partial n_1}{\partial t} = +\frac{1}{\tau_{21}} n_2 + \frac{1}{\tau_{31}} n_3 - \frac{\sigma_{13} I_p}{h\nu_p} n_1 - \frac{\sigma_{31} I_p}{h\nu_p} n_3 - \frac{\sigma_{12} I_s}{h\nu_s} n_1 + \frac{\sigma_{21} I_s}{h\nu_s} n_2, \tag{2.34}$$

where τ_{jk} and , σ_{jk} are the lifetime and the cross section of the relevant states respectively, n_{j} is the relative population of j^{th} level and $I_{\mathrm{s,p}}$ is the intensity of signal or pump. By neglecting the n_3 since the transitions from 3^{th} level to 2^{nd} level are very fast, the equations are simplified to

$$\frac{\partial n_2}{\partial t} = -\frac{1}{\tau_{21}} n_2 + \frac{\sigma_{13} I_p}{h\nu_p} n_1 + \frac{\sigma_{12} I_s}{h\nu_s} n_1 - \frac{\sigma_{21} I_s}{h\nu_s} n_2 \tag{2.35}$$

$$\frac{\partial n_1}{\partial t} = +\frac{1}{\tau_{21}} n_2 - \frac{\sigma_{13} I_p}{h\nu_p} n_1 - \frac{\sigma_{12} I_s}{h\nu_s} n_1 + \frac{\sigma_{21} I_s}{h\nu_s} n_2. \tag{2.36}$$

Practically, the population levels of states of a resonator are not very convenient quantities, therefore one can normalize the equations to the roundtrip amplitude gain $g(\omega) = \sigma(\omega)(N_2 - N_1)$ experienced by the light and the circulating intracavity power $P = I \cdot A_{\mathrm{eff}}$:

$$\frac{\partial P}{\partial t} = \frac{g - l}{T_R} P, \tag{2.37}$$

$$\frac{\partial g}{\partial t} = \frac{g - g_{\text{ss}}}{\tau_g} - \frac{gP}{E_{\text{sat}}}, \tag{2.38}$$

where, T_R is the cavity round-trip time, l is the cavity loss, g_{ss} is the small-signal gain (for a given pump intensity), τ_{g} is the gain relaxation time (often close to the upper-state lifetime), and E_{sat} is the saturation energy of the gain medium. One can solve the equations for gain in steady state and find

$$g = \frac{g_0}{1 + \frac{P_{\text{s}}}{P_{\text{sat}}}} \tag{2.39}$$

and if frequency dependence is also added (Lorentzian shape for instance), then the equation becomes:

$$g(\omega) = \frac{g_0}{1 + (\omega - \omega_a)^2 \tau_2^2 + \frac{P_{\text{s}}}{P_{\text{sat}}}}, \tag{2.40}$$

where ω_a is the atomic transition frequency and τ_2 is the dipole relaxation time. Thus, when the gain is added to the nonlinear Schroedinger equation, it can be written as

$$\frac{\partial a}{\partial z} - i\frac{1}{2k_0}(\frac{\partial^2}{\partial x^2} + \frac{\partial^2}{\partial y^2})a + i\frac{(k_2 + ig\tau_2^2)}{2}\frac{\partial^2 a}{\partial \tau^2} + \frac{l - g}{2}a = i\frac{2\pi n_2}{\lambda_0}|a|^2 a. \tag{2.41}$$

As seen from the equation, gain effects not only the amplitude but also the temporal shape of the pulses since it depends on the frequency. This equation represents how optical pulses propagate inside a waveguide. How the pulses are created inside a laser cavity will be the main topic of the next section.

2.4 Mode-locking of Lasers

Mode-locking of a laser is a method to produce pulses of light of extremely short duration. One of the fundamental parts of the laser is the cavity which determines the allowed modes of the laser by its geometry. For instance, in case of a loop-shape cavity, the modes should obey the periodic boundary conditions of the loop to survive inside the cavity. The principle of mode-locking is to induce a fixed phase relationship between the allowed modes of the laser's resonant cavity such that interference between these modes causes the laser light to be produced as a train of short pulses. There are two types of mode-locking: active mode-locking and passive mode-locking. All of the studies using ultrafast pulses reported in this thesis utilize passive mode-locking, specifically "nonlinear polarization evolution". A nice overview of active and passive mode-locking techniques are in reference cited [5].

Passive mode-locking is achieved by engineering the parameters of the cavity such that the light will be favored to form pulse trains. By optimizing the dispersion, nonlinearity, gain and nonlinear loss parameters, one can create various attraction points of the cavity such as continuous-wave lasing, soliton shape pulses, similariton shape pulses, *etc...* The noise initially created by the spontaneous emission of the gain medium, will evolve toward that attraction point in each roundtrip to survive inside the cavity. For creation of pulses, adding a fast saturable absorption or similar effects inside the cavity is the one of the most common methods [6]. The principle is to give some loss to the light with respect to its instantaneous power (lower loss for higher power) in each roundtrip of the cavity. Thus, the cavity parameters behave like favoring the light to be collected in time domain and form pulses to survive. In frequency domain, the light that has allowed frequencies by the cavity length and appropriate phases to form interference pattern of pulse train can survive after millions of roundtrips. The others are either absorbed by saturable absorber or extracted from the cavity.

Nonlinear polarization evolution (NPE) supplies the fast saturable absorber condition by making use of the intensity dependent changes in the state of polarization when the orthogonally polarized components of a single pulse propagate inside an optical fiber [7]. Due to the nonlinear Kerr phase shift, the polarization of the intense center of the pulse is rotated further than the less intense wings, Figure 2.3. In order to understand the working principle of NPE, let us start from the polarizing beam splitter output. The linearly polarized light enters the quarter wave plate and it changes the polarization slightly towards elliptical. The reason is to increase the effect of Kerr nonlinearity inside the cavity. After the fiber section, the polarization of the pulse peak point will be different from the polarization of the wings, since the instantaneous power differs. The polarization is changed to linear polarization again in the quarter waveplate and turned

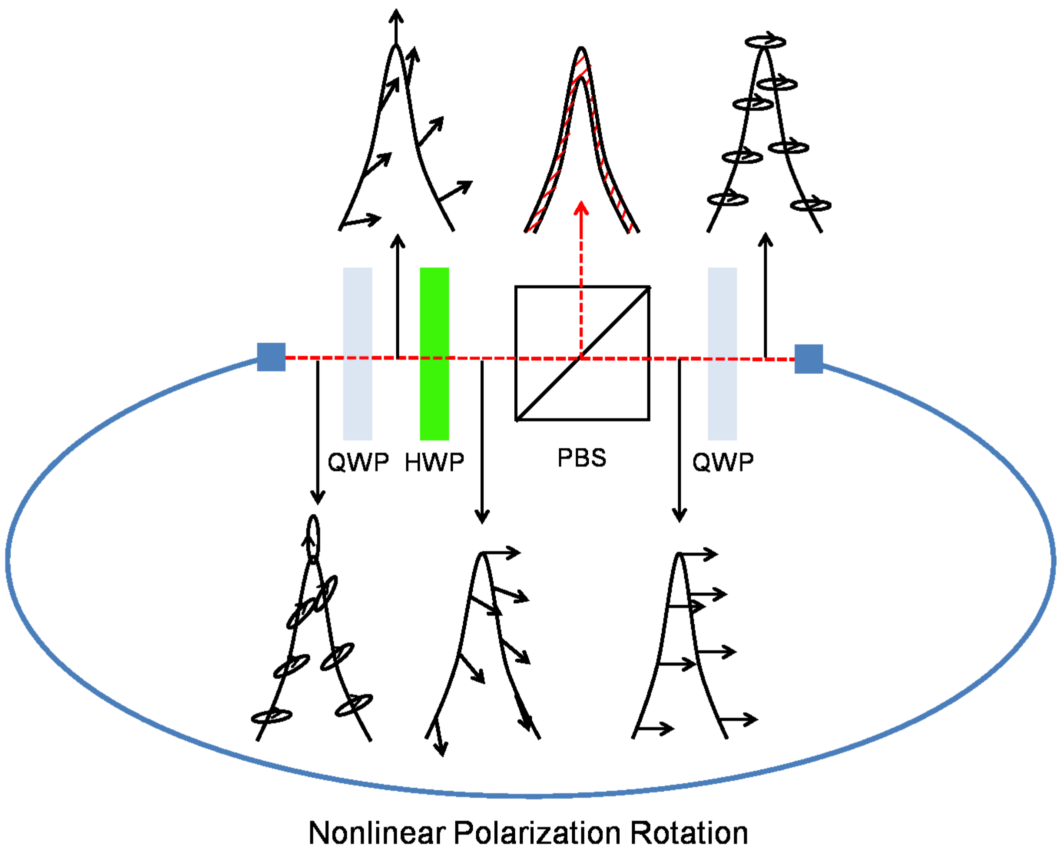

Figure 2.3: Schematic description of nonlinear polarization evolution.

ninety degrees in the half wave plate to make the most shifted (most powerful) parts remain inside the cavity. The other parts will be extracted from the cavity reversely proportional to their power. The total effect of the waveplates, fiber and polarizing beam splitter is a shortening of the pulse after each round trip acting like a fast saturable absorber.

The master equation should also cover the fast saturable absorber effect to be a complete driving equation of ultrafast pulse propagation. The formula for the fast saturable absorber can be written as [6]

$$q\left(A\right) = \frac{q_0}{1 + \frac{|A|^2}{P_{\mathrm{A}}}} \tag{2.42}$$

or

$$q\left(A\right) = q_0 \cos\left(\frac{\left|A\right|^2}{P_\mathrm{A}}\right). \tag{2.43}$$

The first equation is used for semiconductor saturable absorber mirror (SESAM) where the second one is used for nonlinear polarization evolution. But both of them have the same terms if the absorber is not saturated:

$$q\left(A\right) = q_0(1 - \frac{\left|A\right|^2}{P_\mathrm{A}}), \tag{2.44}$$

where q_0 is the modulation depth and P_A is the saturation power. The first term, unsaturated linear loss can be absorbed in the cavity losses $l' = l + q_0$. When the second term is added to the master equation it becomes:

$$\frac{\partial a}{\partial z} - i\frac{1}{2k_0}(\frac{\partial^2}{\partial x^2} + \frac{\partial^2}{\partial y^2})a + i\frac{(k_2 + ig\tau_2^2)}{2}\frac{\partial^2 a}{\partial \tau^2} + \frac{l-g}{2}a - \frac{q_0}{P_A}\left|a\right|^2 a = i\frac{2\pi n_2}{\lambda_0}\left|a\right|^2 a. \tag{2.45}$$

There is no analytical solution of this equation and simulations based on finite difference method are mostly used to analyze the solutions. There are huge variety of the parameters (gain, loss, dispersion, nonlinear coefficient) which determines the working regime of the laser.

Soliton pulse shape is one of the main solutions of the master equation [8, 9]. Soliton laser requires all negative dispersion in all part of the cavity. Soliton pulses behave like eigenfunction of the equation and preserve their shape, width and power inside the cavity. The pulse energy of soliton fiber lasers are usually limited to ~100 pJ level due to the nonlinear effects.

A similariton laser produces parabolic shape pulses which preserve its shape under positive dispersion and nonlinearity [10, 11]. The pulse width increases through the cavity and should be shortened in a negative dispersion part to meet the periodicity condition. The similariton lasers can go up relatively higher pulse energies since the instantaneous power is not at the peak value in all around the cavity.

In the dispersion-managed lasers, the dispersion of the cavity is managed such that the cumulative effect on the pulse in each single round trip mimics the parameters of fundamental solutions. The cavity total dispersion can be negative zero or positive. For net-negative dispersion cavities, the laser is called dispersion managed soliton lasers, and they behave like solitons in average [12]. Highly positive dispersion managed lasers, called all-normal dispersion laser and the pulses should be filtered to supply the periodicity [13]. Dispersion-managed lasers with near-zero net cavity dispersion can produce pulses with very broad spectrum and can be compressed outside the cavity to obtain very short pulses.

A soliton-similariton laser is a hybrid laser where in the one half of the laser, parameters push the pulses toward soliton shape, but in the other half toward similariton shape [14]. Since there are two strong attraction points more stable pulses are produced with that design.

In all these mode-locking regimes it is assumed that there is only one pulse inside the cavity and the periodicity is for one roundtrip. The master equation supports multiple-pulse formation and period doubling but they are not being considered as fundamental regimes. Although they can sometimes be used to produce pulse trains with variable repetition rate (bound pulses *etc...*), we consider them as instabilities of the mode-locked lasers in this thesis.

Chapter 3

Intensity Noise of Mode-locked Fiber Lasers

3.1 Introduction

In the field of mode-locked fiber lasers, prior to 2003 a rapid progress have been reported with limited pulse energies around 1-3 nJ. Recently, it has been reported that for 80 fs pulses, the pulse energies have reached the level of 30 nJ [15]. Such lasers exhibit complex dynamics arising from the coaction of strong nonlinear, dispersive, and dissipative pulse shaping effects altogether [16]. In addition to the well-known soliton-like and stretched-pulse (dispersion-managed soliton) regimes, several distinct mode-locking regimes have also been recently identified such as similariton, all-normal dispersion, and soliton-similariton. As a result of increasing pulse energies generated by these laser systems, the question of their noise performances arises. Many of the applications using mode-locked fiber laser systems; such as spectroscopy, metrology, free electron laser based accelerators and laser-material interactions; are influenced by the laser intensity noise. Particularly while seeding a chain of amplifiers, laser noise becomes crucial [17]. On the other hand, it is not easy to discern changes in the noise level through the usual pulse characterization methods.

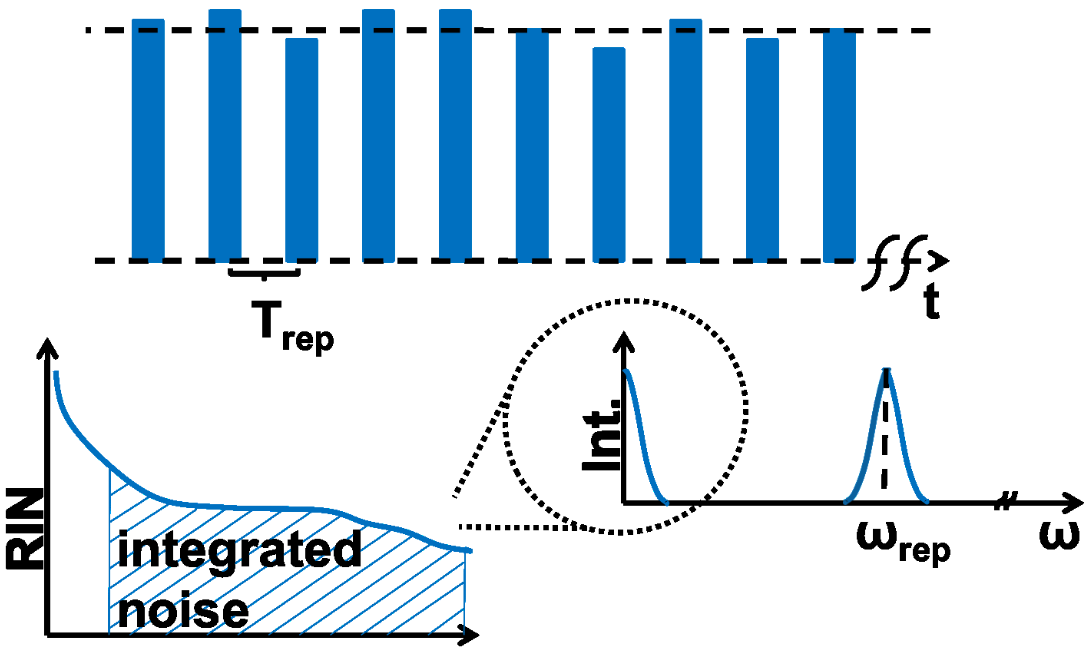

Figure 3.1: Relative intensity noise.

To the best of our knowledge, there is not any systematic characterization of the noise performance of mode-locked fiber lasers available. The laser noise has been investigated theoretically using an emphasis on timing jitter [18, 19], several studies on a particular fiber laser design include characterizations of oscillator [20, 21, 22, 23] and amplifier noise [23, 24]. Nevertheless, it has not been identified, how the noise performance varies over the rich variety of pulse-shaping schemes and the vast accessible parameter ranges. In this chapter, a systematic characterization of intensity noise of mode-locked fiber lasers are reported for a wide range of parameters. The results of this study have been published in Optics Letters [25].

Intensity noise is the power fluctuation of a laser and the relative intensity noise (RIN) is the noise relative to the laser power (Figure 3.1).

$$P(t) = \bar{P} + \delta P(t) \tag{3.1}$$

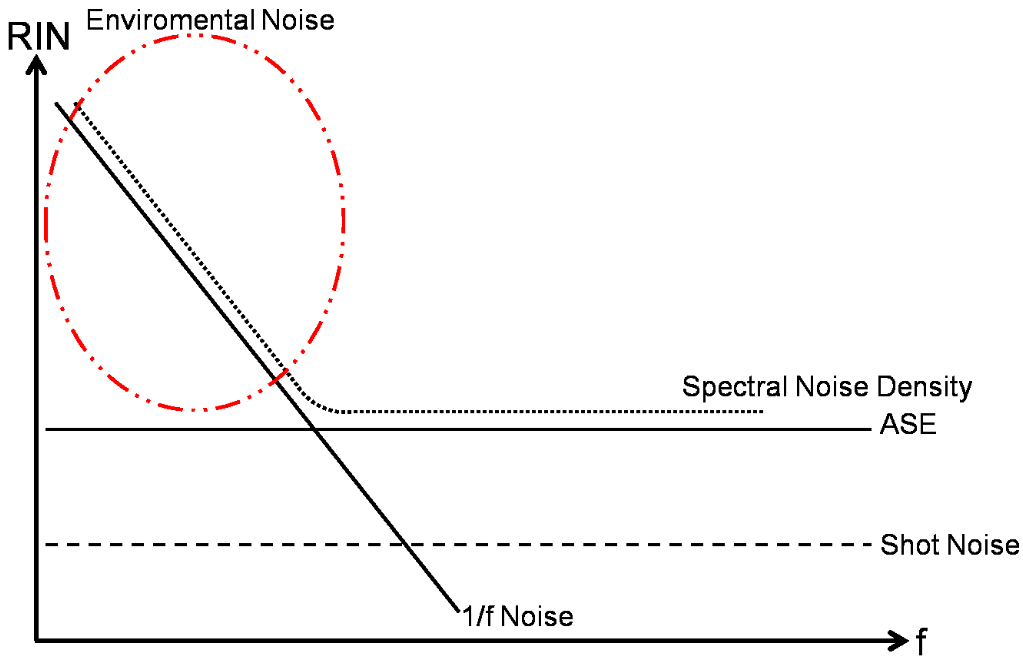

Figure 3.2: Spectral noise density.

$$RIN = \frac{\delta P(t)}{\bar{P}} \tag{3.2}$$

The statistical description of the relative intensity noise is the spectral noise density, which is the Fourier transform of the autocorrelation function of the intensity noise (Figure 3.2).

$$S(f) = \frac{2}{\bar{P}^2} \int_{-\infty}^{\infty} \langle \delta P(t)\, \delta P(t+\tau) \rangle \, exp\,(i2\pi f \tau) d\tau \tag{3.3}$$

The unit of the spectral noise density is $1/Hz$ and the value represents the normalized noise in 1 Hz measurement bandwidth (1 second time window). For measurements longer than 1 second, this value should be multiplied by the reciprocal of the measurement time (measurement bandwidth) in order to find the absolute noise.

$$RIN_{\text{rms}} = \frac{\delta P}{\bar{P}}_{rms} = \sqrt{\int_{f_1}^{f_2} S\left(f\right) df} \tag{3.4}$$

This root-mean-square (rms) RIN value represents the noise per part of the laser power for a 1 second measurement time. In this thesis the reported integrated noise percentages are calculated by multiplying the rms RIN by 100 and all of the given values are obtained for 1 second measurement time.

There are three main sources of the RIN of a fiber laser. One of them is the diode laser which is used as a pump source. The details of how pump noise couples to the laser power are given in the next chapter. Especially the low frequency noises couple due to the $1/f$ noise of the pump diode. In the higher frequencies RIN is limited by the shot noise. Shot noise occurs due to the quantum nature of both light and current and in addition being a white noise. Both the pump diode and photodetector which are used for noise measurements are sources of shot noise. The second source of the RIN is the gain medium itself. Amplified spontaneous emission of the gain medium creates white noise and dominates the spectral noise density in high frequencies. The last source of RIN is the environmental noise, like mechanical, thermal fluctuations that affect the coupling efficiencies of the components of the laser. This occurs in the very low frequency range of the spectral noise density and mostly ruins the long term stability of the laser power, given in Figure 3.2.

3.2 Experimental Setup

For this purpose, we have constructed a specially designed a Yb-doped fiber laser capable to switch easily between soliton, stretched-pulse, similariton, and all normal dispersion regimes, leading us to obtain systematic results (Figure 3.3). All the main results were qualitatively verified using an Er-doped fiber laser [14] and several other Yb-fiber lasers in our laboratory. The cavity of the primary laser used in this study is similar to those reported in [10, 11], comprised of 60 cm long highly doped Yb-fiber, approximately 450-cm-long single-mode fiber (SMF), and

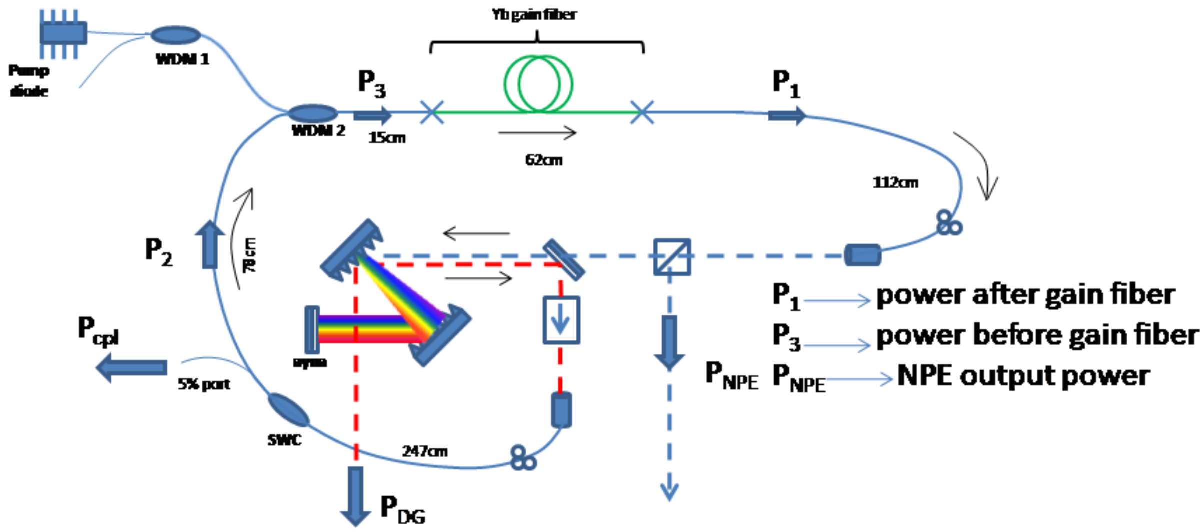

Figure 3.3: Scheme of the fiber laser under test.

a freespace section. All the fibers have normal groupvelocity dispersion (GVD) 24 fs^2/mm. The total cavity dispersion is controlled with a pair of diffraction gratings (GVD of 0.0141 ps^2/cm). For allnormal dispersion operation, the grating compressor is replaced by a bandpass filter of 10 nm bandwidth. The repetition rate varies between 35 and 40 MHz, depending on the particular configuration. Mode-locking is achieved by nonlinear polarization evolution (NPE) [7]. Measurements are taken from the polarization rejection port, the 5% fiber coupler, and the reflection of the first diffraction grating, such that power levels at every point throughout the laser cavity can be deduced.

The standard method is used for the RIN characterization [26] (Figure 3.4). The optical signal is detected using an InGaAs photodiode. The signal which is obtained by low-pass filtering (dc to 1.9 MHz) the photocurrent at baseband is analyzed using a high dynamic range baseband spectrum analyzer with a bandwidth of 250 kHz. In order to obtain the integrated noise, the noise spectrum is integrated, multiplied by 2 (to account for the double sidebands), and the square root over the desired bandwidth is taken. The mode-locking characteristics have been established by long-range autocorrelation, optical, and rf (12 GHz

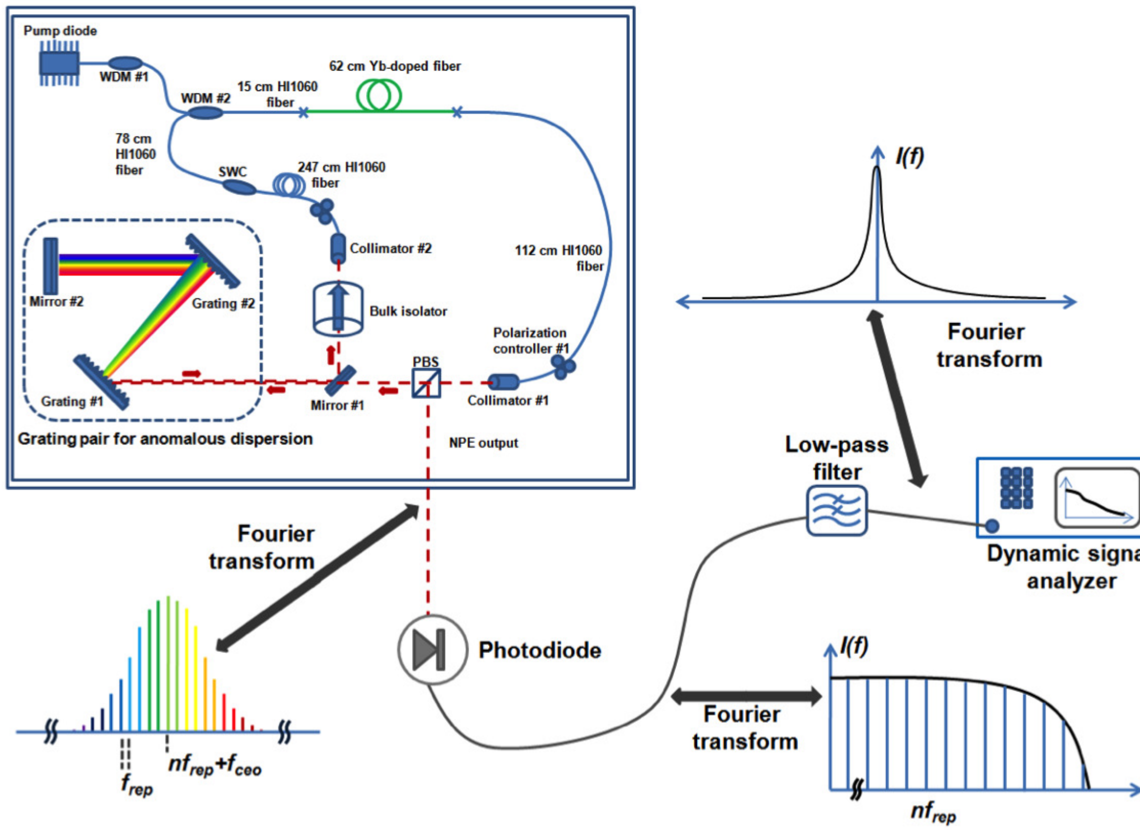

Figure 3.4: Experimental setup for RIN measurements.

bandwidth) spectra measurements.

3.3 Results

During the systematical characterization of intensity noise of mode-locked fiber lasers for all major mode-locking regimes, a wide range of parameters have been applied. The obtained results reveal that equally low-noise performance can be obtained for all regimes. Losses taking place inside the cavity influence noise strongly without a clear trace in the pulse characteristics. It has been reported that the high-energy fiber laser oscillators obtained up to date have utilized large output coupling ratios, and they are likely to have high noise. Instabilities which

Laser	GVD (ps^2)	RIN-LO (%)	RIN-HI (%)
5 A	- 0.070	0.028 (2.6 nJ)	0.029 (5.2 nJ)
B	+ 0.005	0.029 (2.8 nJ)	0.030 (5.3 nJ)
C	+ 0.020	0.028 (2.8 nJ)	0.029 (5.6 nJ)
D	+ 0.100	0.023 (3.2 nJ)	0.023 (5.8 nJ)

Table 3.1: Lowest integrated (from 2.9 Hz to 250 kHz) RIN values at a low (RIN-LO) and a high (RIN-HI) pulse energy. A: soliton-like laser; B: stretched-pulse laser; C: similariton laser; D: all-normal dispersion laser.

occur at high pulse energies are characterized. Below a threshold value for the onset of nonlinearly induced instabilities, the noise level is virtually independent of pulse energy. In this region, continuous-wave peak formation and multiple pulsing only moderately influence the noise performance. However, for high energies, a noise outburst is encountered, resulting up to 2 orders of magnitude increase in noise. These results effectively constitute guidelines for minimization of the laser noise in mode-locked fiber lasers.

Initially, the noise performance of pump diodes from three different vendors has been tested, which yielded similar results for all power levels. The RIN of the laser has been characterized over different mode-locking regimes and over the entire pump power range where mode-locking can be maintained. Thus, we have been able to systematically investigate the effects of the (i) mode-locking regime, (ii) cavity finesse (*i.e.*, losses), and (iii) pulse energy, including nonlinearly induced instabilities.

While switching between different mode-locking regimes, the minimum noise state for each regime has been searched by varying the pump power, fine tuning cavity dispersion, and by adjusting the wave plates which control the NPE; yielding nearly the same noise levels for the soliton, similariton, stretched pulse, and all-normal dispersion regimes, given in Table 3.1. We believe that the marginally lower RIN of the all-normal dispersion regime is simply because high losses at the grating compressor are avoided.

The finesse of the cavity is an important parameter, which determines the amplification factor per round trip. An increase in the gain leads to increase in noise

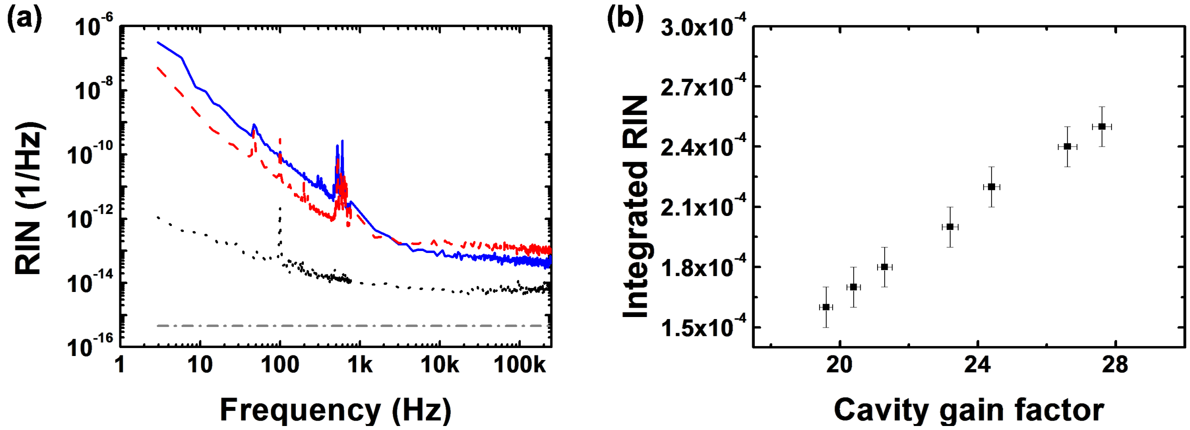

Figure 3.5: (a) Measured noise spectrum corresponding to highest (solid, blue line) and lowest (dashed, red line) cavity finesse levels obtained by adjustment of the linear loss. Dotted (black) line shows the measurement noise floor. Dash-dotted (gray) line indicates the shot noise limit. (b) Corresponding RIN of the laser integrated over the frequency range 2.9 Hz - 250 kHz, as a function of the net gain through the amplifying fiber segment.

level as a result of increased amplified spontaneous emission [27, 28]. Keeping pump power and polarization settings fixed, losses of the cavity have been varied by using a variable output coupler, which is composed of an additional half-wave plate positioned behind the polarizing beam splitter cube, and the diffraction gratings acting as a polarizer. Over the range losses which can be adjusted without losing mode-locking, we have found the total RIN to increase linearly with increasing cavity losses, given in Figure 3.5. The output power measured from the polarization port can be controlled through the polarization parameters, for lasers employing NPE. In order to minimize the nonlinear effects, it is common practice to maximize the pulse energy by increasing the power coupled out. The effect of the finesse is investigated by adjusting the NPE parameters under constant pump power and the total RIN is again found to increase up to 1 order of magnitude with increasing NPE output coupling, given in Figure 3.6. In other words, the noise performance deteriorates due to increased power extraction, both from a linear port and the NPE port. These results quite significantly imply that many of the previously reported high-energy fiber lasers are likely to have been

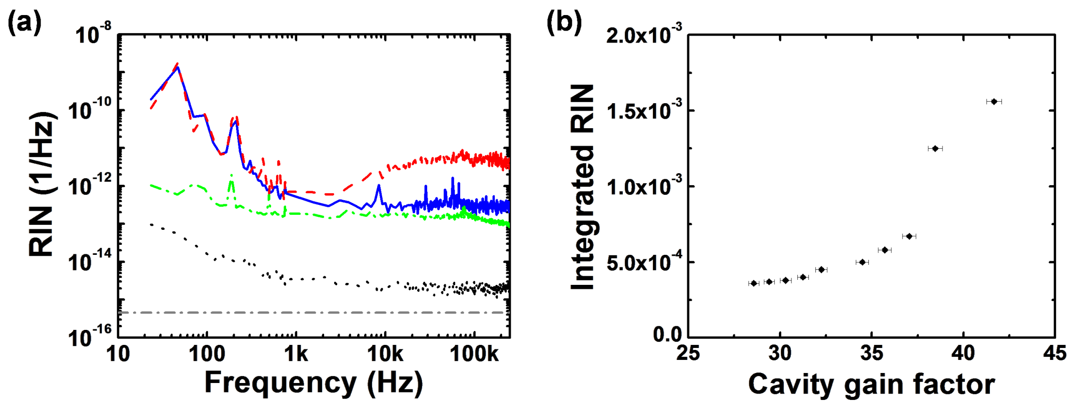

Figure 3.6: (a) Measured noise spectrum corresponding to highest (solid, blue line) and lowest (dashed, red line) cavity finesse levels obtained by adjustment of the NPE loss. Dash-dotted (green) line shows the typical noise spectrum of the pump diode. Dotted (black) line shows the measurement noise floor. Dash-dotted (gray) line indicates the shot noise limit. (b) Corresponding RIN of the laser integrated over the frequency range 2.9 Hz - 250 kHz, as a function of the net gain through the amplifying fiber segment.

relatively high-noise lasers.

A natural question is how the noise performance depends on the pulse energy for a given cavity finesse. Although it is difficult to make controlled experiments over a broad range of pulse energies owing to the finite stability window, measurements indicate that up to a critical pulse energy, noise performance remains constant, irrespective of the mode-locking regime (Table 3.1). However, beyond the critical energy, where the precise value of which differs from laser to laser, instabilities induced by nonlinear effects are encountered. The formation of a continuous-wave (cw) peak on the spectrum and multiple pulse formation are well known. Although cw peak formation is undesirable, the overall intensity noise of the laser is not increased by much; for example, the emergence of a cw peak in the stretched-pulse regime (2.8 nJ of intracavity pulse energy) leads to an increase of integrated RIN by 25% of its value without cw peak formation (Figure 3.7(a)). The highest increase we have observed was by a factor of 2. We find that the effect of multiple pulsing is similar. The Er-doped fiber laser exhibits

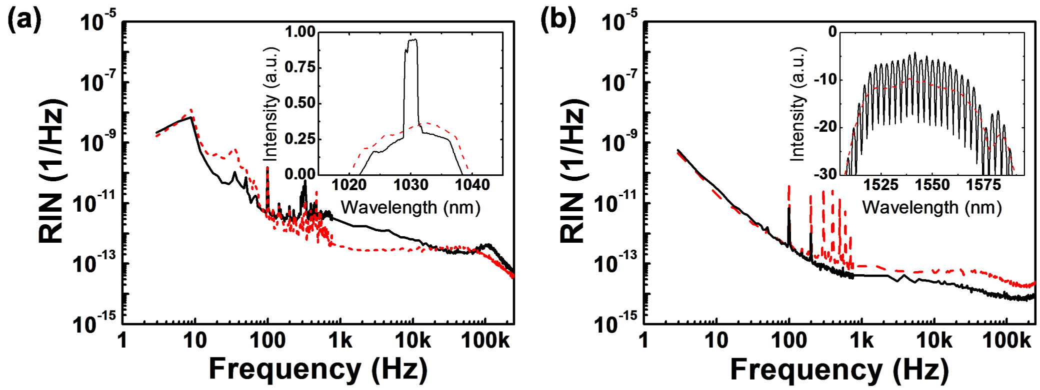

Figure 3.7: (a) Laser noise spectrum with (solid, black line) and without (dashed, red line) cw peak. Inset shows the measured optical spectra with (solid, black line) and without (dashed, red line) cw peak. (b) Laser noise spectrum for double-pulsed (solid, black line) and single-pulsed (dashed, red line) operation. Inset shows the measured optical spectra for double-pulsed (solid, black line) and single-pulsed (dashed, red line) operation.

multiple pulsing more readily. A typical case is shown in Figure 3.7(b), where the integrated RIN during bound pulsing (pulse-to-pulse spacing of 3 ps, combined intracavity pulse energy of 1.7 nJ) increases by 40% of its value without multiple pulse formation.

As the pulse energy is increases beyond a threshold, the laser can experience a noise outburst without cw peak formation or multiple pulsing. We observed this behavior for the soliton and stretched-pulse regimes in this study. The precise value of the threshold depends on the laser configuration. The high-noise state has nearly 2 orders of magnitude higher integrated RIN. Once in the high-noise state, power has to be reduced to a lower threshold to switch back to the low-noise state, tracing a clear hysteresis curve (Figure 3.8 (a)). Switching between the states is abrupt (initiated over a change of power by 1%). With the possibility of an environmental effect or pump diode instability ruled out, these observations are characteristic of a strongly nonlinear system undergoing relaxation oscillations [29]. As a practical matter, we note that it may be difficult to discern if a

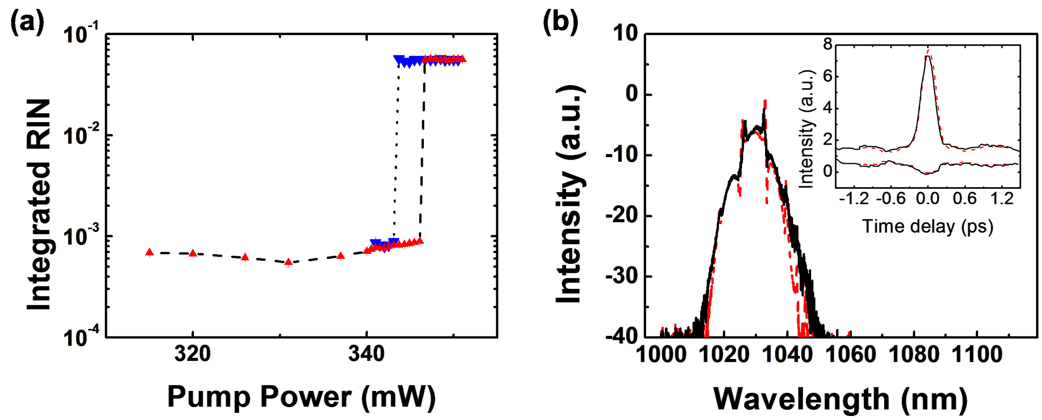

Figure 3.8: (a) Integrated (from 2.9 Hz - 250 kHz) RIN of the laser, as the pulse energy is first increased (red, upward triangles) and then decreased (blue, downward triangles). (b) Optical spectra and autocorrelation traces (inset) measured immediately before and after the transition are shown by dashed (red) and solid (black) lines, respectively.

given laser is in such a high-noise state, as the autocorrelation, optical spectrum measurements look indistinguishable from normal operation. Only in some of the cases we have seen that a high-dynamic range optical spectrum measurement reveals indications of increased noise (Figure 3.8 (b)).

3.4 Conclusion

In conclusion, we report a systematic investigation of the intensity noise of passively mode-locked fiber lasers with the following main result: (1) Noise level appears to be independent of the mode-locking regime. (2) Higher cavity finesse minimizes noise. Consequently, maximizing energy extraction by increasing the output coupling ratio has a detrimental effect on the noise performance. Most high-energy lasers reported thus far may have had a relatively poor noise performance. (3) Well-known indicators of instability, such as the formation of a cw peak or onset of multiple pulsing, lead to relative increases in noise of $30\% - 200\%$

only. (4) An outburst of noise is encountered when a threshold in pulse energy is exceeded. Although further work is needed to fully understand this phenomenon, it appears to result from the coupling of nonlinear effects to noise. It is remarkable that noise processes occur on a microsecond time scale, whereas nonlinear pulse shaping acts on a much faster (fs-ps) time scale. The lowest noise values reported here are comparable to the best performances reported for Ti:sapphire lasers [26]. Furthermore, it can be concluded that extracting pulses in moderate power levels and amplifying them is a better method than directly extracting high power pulses from a laser in terms of noise performance.

Chapter 4

Intensity Noise of Fiber Amplifiers

4.1 Introduction

The relative intensity noise of the fiber lasers is reported in the previous chapter. However, laser power directly extracted from the oscillator is not sufficient for most of the applications. Using a chain of amplification stages is a common method to achieve desired high laser powers. For material processing or nano-surgery, where high laser power is necessary, intensity noise determines the ultimate limit of resolution. Furthermore, in sensing applications intensity noise affects the signal to noise ratio of the measurement. Thus, for most of the high power applications, intensity noise is very important, and the noise created in the amplification stage determines the final noise performance of the high power laser systems. In this chapter, we report a fiber laser system where the amplifiers are seeded by ultra-low intensity noise pulses. The experiences gained from the laser noise research is used to increase the noise performance of the seed laser and the noise added during amplification is analyzed. The system is mostly constructed by Kıvanç Özgören and Pranab Mukhopadhyay, and the noise optimization of the seed source and noise characterization of the system is done by the author.

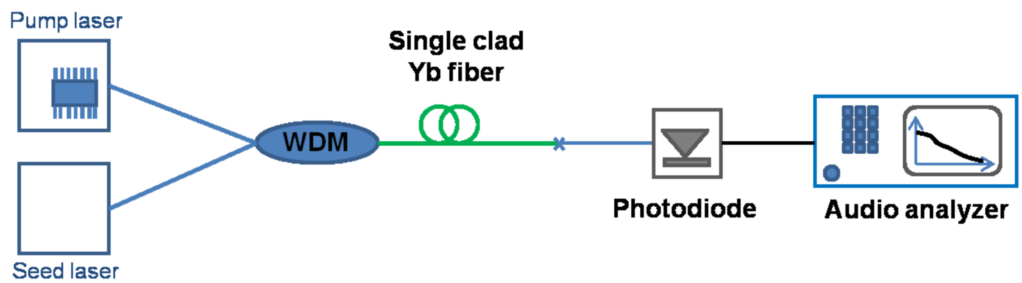

Figure 4.1: Scheme of a fiber amplifier and noise measurement.

The results of this study have been published in IEEE Journal of Selected Topics in Quantum Electronics [23].

In a conventional scheme of a fiber amplifier, the gain medium is optically pumped by a diode laser. The seed signal and pump signal are combined in the gain fiber with a signal-pump combiner or a wavelength division multiplexer. The signal is amplified through the gain fiber with stimulated emission (Figure 4.1) [30].

There are four main sources of the RIN of a fiber amplifier. The main difference from the sources of fiber laser is the noise coupling from the seed signal. Since there is no seed signal in fiber lasers, it is an extra source for amplifiers. The other three noise sources (pump noise, spontaneous emission, and environmental noise) also exist for amplifiers. For high power amplifiers multimode pump diodes are used as pump sources and the noise of such diodes are one or two orders of magnitudes worse than the single mode diodes. Furthermore, laser noise dynamics are more complicated due to the oscillatory nature of the laser cavities. The noise coupling from the pump source and seed source will be examined in more detail in the next chapter. Last, environmental noise may ruin the long term stability performance of the high power systems due to the heating of the components of the system, but in this thesis the short term noises are analyzed on which the environmental noise does not dominate.

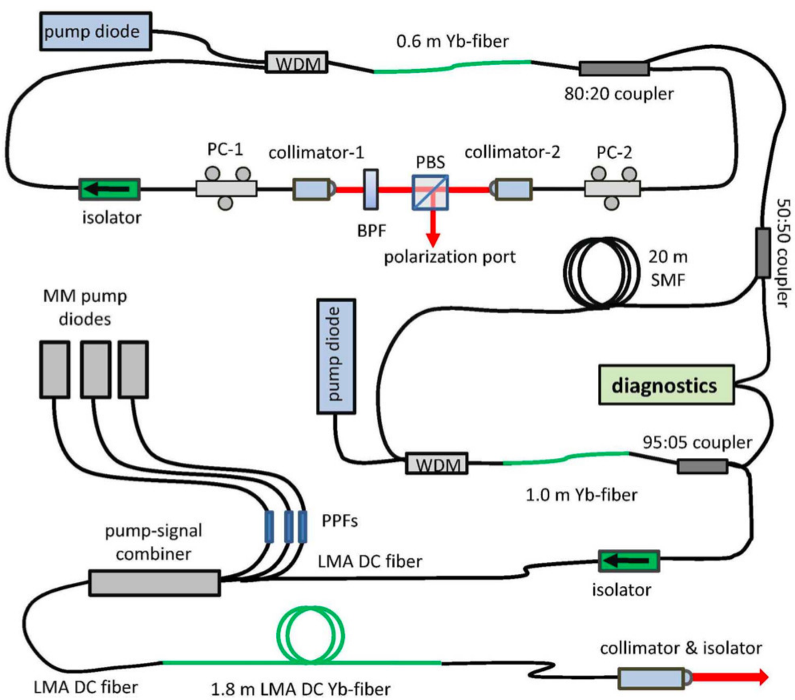

Figure 4.2: Schematic of the laser setup: BPF: band-pass filter, PBS: polarizing beam splitter cube, PC: polarization controller, LMA: large-mode-area fiber, DC: double-cladding fiber, SMF: single-mode fiber, PPFs: pump protection filters, WDM: wavelength-division multiplexer.

4.2 Experimental Setup

The high power laser system under test is an all-fiber amplification system, which consists of a Yb-doped fiber laser, a pulse stretcher region, a pre-amplifier and amplifier stages (Figure (4.2)). The laser works in all-normal dispersion mode-locking regime. The gain section is 0.6 m of highly Yb-doped gain fiber (core diameter of 6.2 m, 0.14 NA, 500 dB/m absorption at 976 nm) which is pumped in-core by a fiber-coupled pump laser diode at 976 nm with a maximum optical power of 300 mW. The cavity net group velocity dispersion is around 0.1 ps^2. The nonlinear polarization evolution technique is used to achieve mode-locking with the help of two polarization controllers and one polarization beam splitter cube. A Fabry-Perot filter is also used for all-normal dispersion mode-locking regime operation. An output power of 26 mW at 43 MHz repetition rate and 1060 nm central wavelength is obtained directly through a 20% output coupler after the gain fiber.

After the oscillator, 50% of the power is used for monitoring. The other part is stretched in time domain through a 20-m-long single mode fiber with the help of positive dispersion. Stretching is necessary to decrease the peak power of the pulses, for reducing the nonlinear effects in the amplification stages (chirp pulse amplifier [31]). Preamplification stage is necessary to relax the power requirements from the laser oscillator, since maximizing energy extraction by increasing the output coupling ratio has a detrimental effect on the noise performance of the laser oscillators. The power is increased to 100 mW level in preamplifier. 1-m-long single mode Yb-doped fiber, which is pumped in-core by a 976 nm diode laser, is used as a gain medium.

In the power amplifier section, the gain section consists of 1.8 m-long Yb-doped double cladding large mode area fiber (DC LMA) which is pumped by three 975 nm diodes with 8 W of maximum power. The seed signal and pump laser are coupled to the gain fiber with a 6-port multiple pump and signal combiner (MPC). An in-fiber isolator-collimator is used to collimate the output laser light. Isolator protects the system from backreflection of the laser light.

4.3 Results

The oscillator produces 22 nm bandwidth pulses which correspond to a transform limited pulse width of 132 fs (Figure 4.3(a)). Although the spectrum seems to be highly structured, the rf spectrum is smooth, and there is not any sign of instabilities, like multiple pulse formation or period doubling at the 50% fiber-coupled output of the oscillator. In the 20-m-long single mode fiber stretcher section, the pulse width increases to around 20 ps, where the spectrum remains unaffected. Then the pulses are amplified in the preamplifier section. As seen in the spectrum of the pulses (Figure 4.3 (b)), the bandwidth is increased slightly

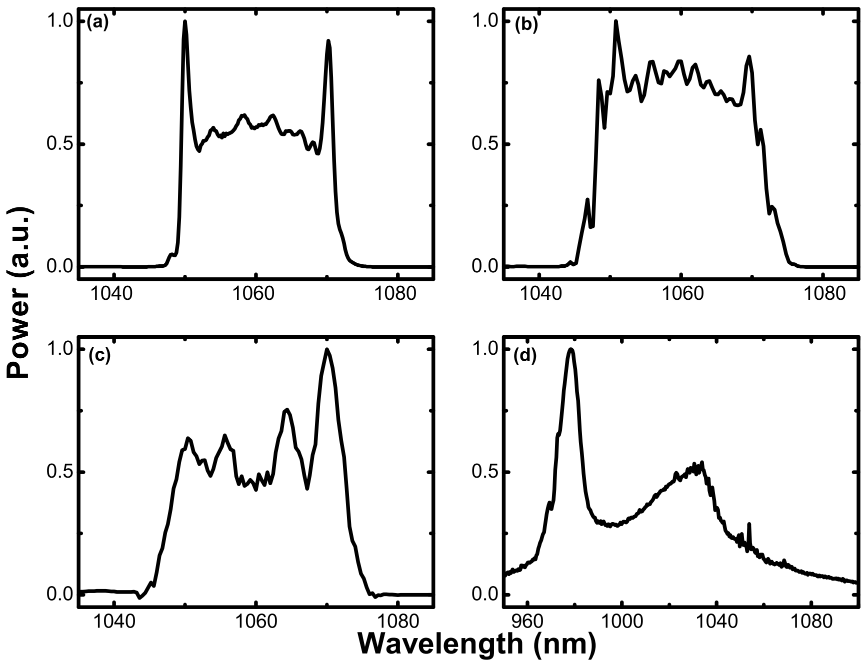

Figure 4.3: Measured spectra obtained from: (a) oscillator output, (b) preamplifier output, (c) amplifier output (at 10.6 W of power), (d) an unused pump port (showing backward propagating ASE signal and residual pump power).

around 1 nm. Furthermore, there can be seen some oscillatory modulations at the edges of the spectrum. The changes in the spectrum are due to the nonlinear effects. There is no sign of amplified spontaneous emission or Raman-shift in the spectrum. The output power of the high power stage is varied by changing the pump power. The optical conversion efficiency is around 50%. The maximum measured output power from the isolator-collimator port is 10.6 W with a total pump power of 20 W. Maximum pulse energy is calculated as 230 nJ with an estimated peak power of 13 kW. There are some oscillatory modulations on top of the output spectrum of high power pulses, given in Figure 4.3 (c). These modulations are due to the beating of two orthogonal polarization states and can be avoided by using polarization-maintaining fibers. Furthermore, backward-propagating spectrum is also recorded from the unused pump ports of the multiple pump and signal coupler. The backward signal consists of backward-propagating amplified spontaneous emission, residual pump light and a small fraction of pulses

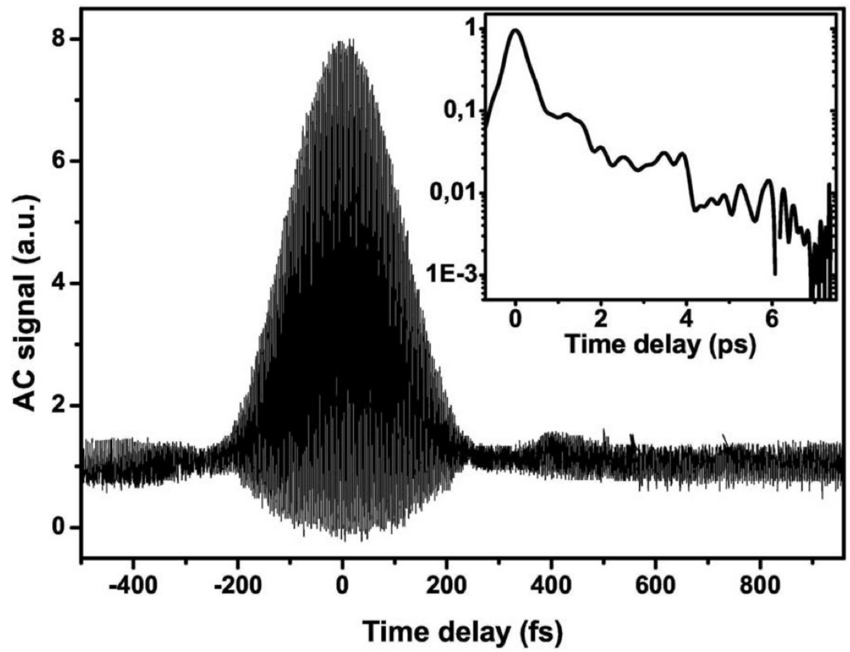

Figure 4.4: Interferometric autocorrelation traces of dechirped pulses at 10.6 W of power. Inset shows the long-range intensity autocorrelation on semi-log scale.

(Figure 4.3 (d)).

Temporal characterization of femtosecond laser pulses cannot be performed with conventional methods since oscilloscopes and photo detectors do not have bandwidths on the order of a few hundred THz. Hence, autocorrelation technique has to be performed in the optical domain using nonlinear optical effects. The setup contains a Michelson interferometer with a variable arm length difference and the original and delayed pulses are interfering in the nonlinear crystal, where frequency doubling is occurring. An autocorrelation graph is obtained by recording the average power of the frequency-doubled signal:

$$I_{ac}(\tau) = \int (E(t) + E(t+\tau))^4 dt. \tag{4.1}$$

The trace of the autocorrelation of the dechirped pulses is shown in Figure

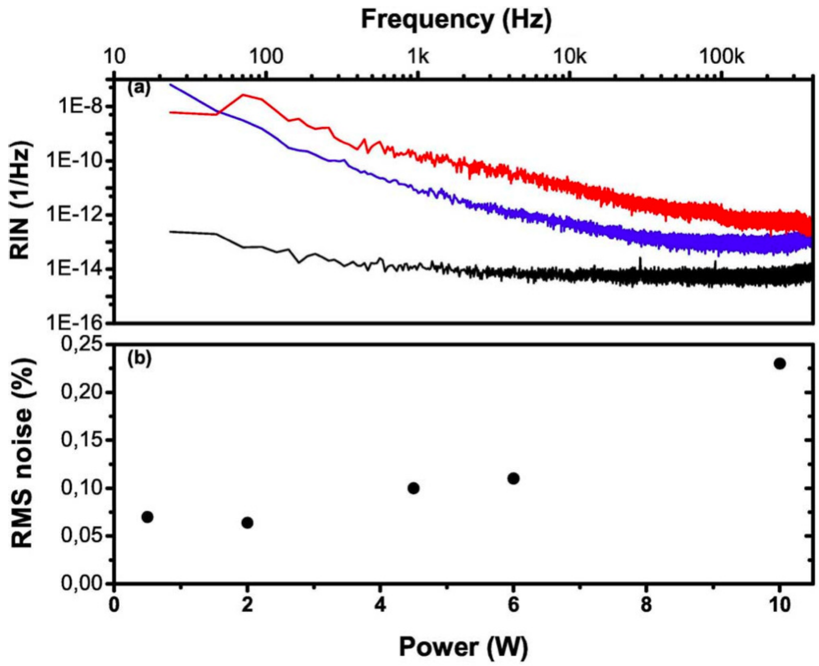

Figure 4.5: (a) Measurement of relative intensity noise (RIN): upper (red) curve is the amplifier RIN at 10.6 W of power, middle (blue) curve is the oscillator RIN, and lower (black) curve is the noise floor. (b) Variation of integrated noise as a function of power in the frequency range of 20-250 kHz. Integrated noise of the oscillator is 0.029% over the same range.

4.4. The data belongs to the pulses at 10.6 W output power. The full-width-half-maximum of the trace is 240 fs, which corresponds to pulse duration of around 160 fs (assuming a Gaussian profile). More than 90% of the energy is under the main curve of the pulse. The long range temporal shape is also shown in the inset of Figure 4.4 to eliminate the multiple pulse formation possibility. Furthermore, no sign of multiple pulse formation is detected based on the rf-spectrum and optical spectrum analyzes.

Figure 4.5 (a) shows the spectral noise density of the pulse train extracted from the oscillator and the amplifier system. The integrated RIN (20 Hz- 250 kHz) of the oscillator is around 0.029%. This noise level is one of the best performances among the fiber oscillators [25]. To achieve this level, the experiences gained from the study of laser noise, which's results are reported in the previous chapter are used: the laser operates in all-normal dispersion mode to decrease the cavity losses, the pump diodes are operated at moderate power level and the extracted power from the laser is kept in optimum level for noise performance. The spectral noise density of the high power amplifier output is also shown in Figure 4.5 (a). It can be seen that the noise increases significantly in the amplifier stage at high powers. The noise density graph is given for the maximum output power 10.6 W, and the integrated noise for different power levels are compared in Figure 4.5 (b). It is shown that the intensity noise of the system is increasing while increasing the output power of the system. Integrated noise for the amplifier output starts from 0.06% at lower power, and goes up to around 0.2% at maximum power of 10.6 W. Since the noise coupled from the seed source is constant in all cases, the decrease in the noise performance can be caused by an increase of the amplified spontaneous emission or the noise coupled from pump diodes. This issue will be reported in more detail in the next chapter.

4.4 Conclusion

In conclusion an all-fiber, high power, low-noise, ultrafast laser system is demonstrated. It is a compact and robust system, since the light goes through the fibers everywhere in the system except the NPE section in the oscillator. The system produces sub-160 fs pulses with 10.6 W average power at 43 MHz repetition rate. It is the first amplifier system that is seeded with all-normal dispersion type laser and operates with noise performance better than the solid state laser systems and comparable to low-noise continuous-wave fiber laser systems [32]. To the best of our knowledge, it is the first study of the characterization of the intensity noise of fiber amplifiers. The system works in its maximum power with a noise performance better than 0.2% where the seed signal's intensity noise is less than 0.03%. The noise increases significantly while increasing the output power of the system It will be discussed in more detail in the next chapter.

Chapter 5

Prediction of Laser and Amplifier Noise From Their Modulation Transfer Functions

5.1 Introduction

The noise of fiber lasers, although typically quite low ($< 0.1\%$), has significant contributions from technical noise, *i.e.*, noise coupled from the environment or pump source. Since these can be eliminated with sufficient care, it is important to identify them. There is no systematic study, to our knowledge, of how fluctuations in pump power are transferred to fiber laser noise. On the other hand, it is a well known technique to modulate the pump laser power to decrease the intensity noise of the laser or lock the carrier-envelope frequency to a better frequency source with long term stability [28]. Thus, it is essential to understand the response of the laser to pump modulations and to measure the cut-off bandwidths for pump modulations. Furthermore, these lasers have rich dynamics, arising from the intricate interplay of the strong nonlinear, dispersive, and dissipating pulse shaping effects. Consequently, more characterization methods are needed to deeply understand the dynamics of the mode-locked fiber lasers. In this chapter we investigate how variations in pump power are coupled to the mode-locked laser power and amplifier power as a function of frequency. A modulation or noise transfer function (MTF) is experimentally measured for both the fiber lasers and amplifiers [33]. Furthermore, how the noise from seed source couples to the amplifier power is also investigated, and a frequency dependent modulation transfer function from seed source to amplifier power is experimentally measured. In addition, the measured modulation transfer functions are used to predict the relative intensity noise of fiber lasers and amplifiers. Most of the results of the chapter are published as a conference proceeding [34] and presented at CLEO 2009 by the author. The study of fiber lasers is mostly done by the author with the help of Kutan Gürel, and amplifiers are mostly done by Kutan Gürel with the help the author.

A modulation transfer function defines how the modulations on the pump signal transfer as a modulation of the laser signal as a function of the modulation frequency. Once the relation is known, it will give an idea about the noise coupling from pump source to laser. We also defined modulation transfer functions of amplifiers for both, the modulation transfer from pump source and seed source as functions of the modulation frequency.

$$MTF\left(f\right)_{\text{pump}} = \frac{Output \quad Modulation \quad Amplitude_{\text{laser}}\left(f\right)}{Input \quad Modulation \quad Amplitude_{\text{pump}}\left(f\right)} \tag{5.1}$$

$$MTF\left(f\right)_{\text{seed}} = \frac{Output \quad Modulation \quad Amplitude_{\text{laser}}\left(f\right)}{Input \quad Modulation \quad Amplitude_{\text{seed}}\left(f\right)} \tag{5.2}$$

5.2 Experimental Setup

In the experiments we have mostly used the Yb-doped fiber laser which is constructed as a test laser for noise characterization and described in detail in chapter 3. To produce the MTF-curve in 1550 nm, we used the Er-doped fiber laser which is constructed by Coşkun Ülgüdür and works in soliton-similariton mode-locking regime. The Er-doped fiber laser is similar to the laser in the literature [14].

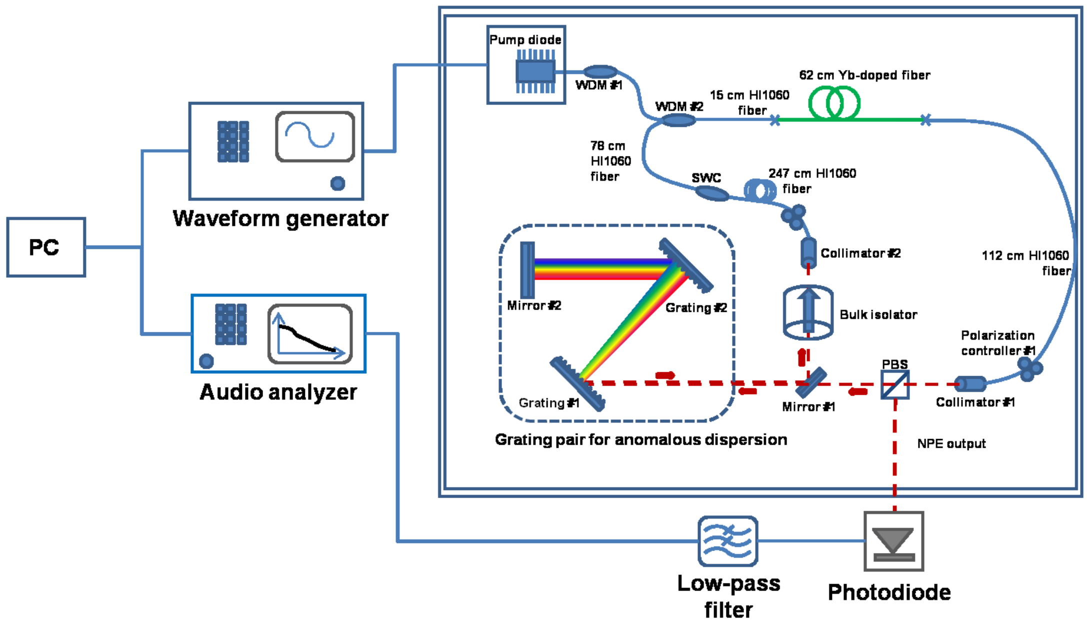

Figure 5.1: Schematic description of MTF measurement of a fiber laser.

The laser pump sources are fiber-coupled distributed feedback diode lasers, which are driven by constant current sources. The pump power is being changed by varying the driving current of the diode lasers. The pump signal is modulated by modulating the driving current of the diodes. In this study, modulation supplies from the modulation input port of the diode driver. The diode driver has a linear modulation transfer function up to a critical modulation current and a plato frequency response in the bandwidth of 1 MHz, which is quite enough for our measurements. Furthermore, there is no resonant frequency within our modulation range. The waveform generator is connected to the diode driver to give the sinusoidal modulation over the frequency range of 1 Hz - 250 kHz, where the upper limit is set by the bandwidth of the noise measurements. The noise is measured by the same method described in chapter 3. In order to find out the modulation transfer ratio of a specific frequency: first the modulation of this frequency on the optical pump signal is measured while the pump diode current is being modulated, then the modulation at the same frequency of the laser output signal is measured at the same frequency and finally the measured amplitude of

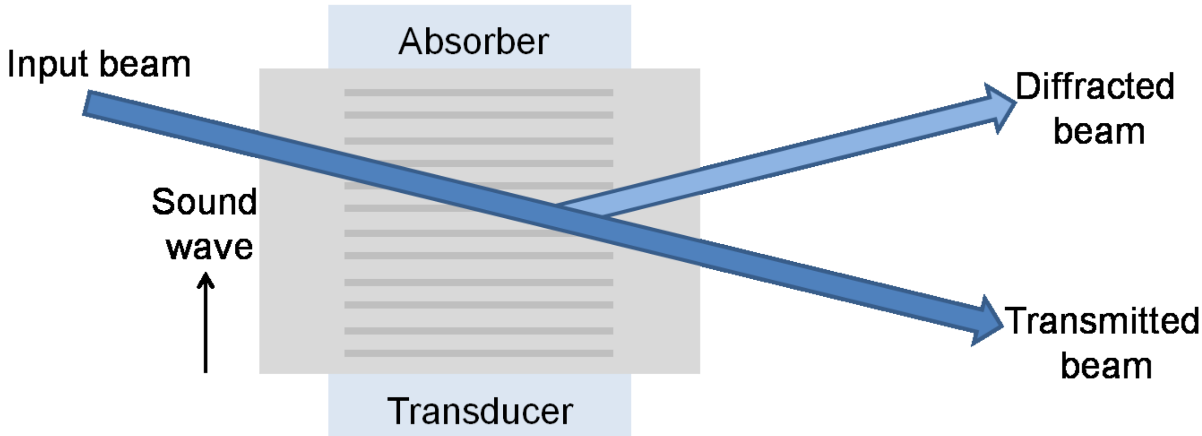

Figure 5.2: Working principle of acousto-optic modulator.

laser modulation is divided by the measured amplitude of the pump modulation at the specific frequency. All the measurements are repeated in the entire frequency range and plot the MTF with respect to modulation frequency (Figure 5.1). The entire measurement is automated via a computer using automation software of LabVIEW.

The experimental setup for MTF measurements of fiber amplifiers is almost the same as the setup for fiber lasers. The only difference is in the measurement of modulation transfer function from the seed signal to the laser. An intensity modulator is used to modulate the seed signal, arising from the seed laser. An acousto-optic modulator (AOM) is used as the intensity modulator. An AOM is an intensity modulator based on the acousto-optic effect, *i.e.* the modification of the refractive index by the oscillating mechanical pressure of a sound wave (Figure 5.2). The same procedure for measuring the modulation transfer function from pump source is applied for the MTF from the seed source, but this time the sinusoidal modulation signal is given to AOM from the waveform generator (Figure 5.3).

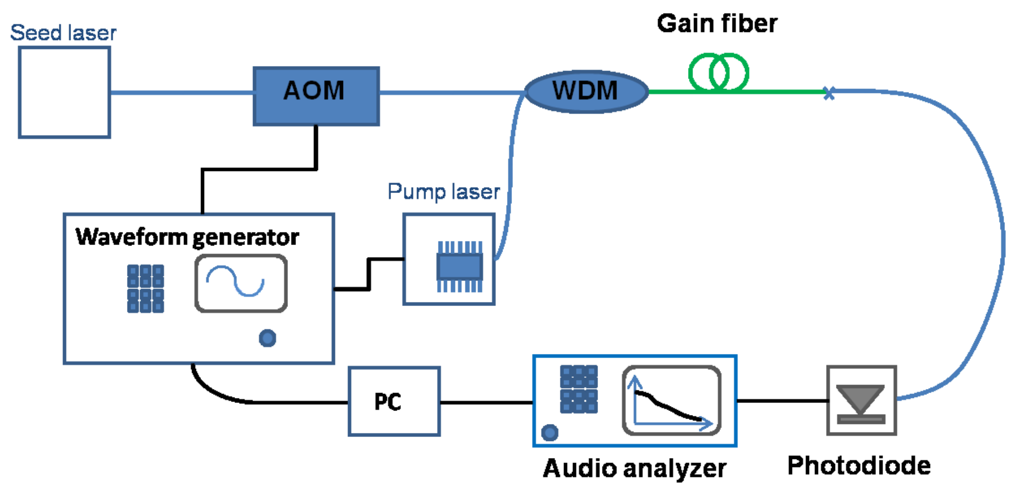

Figure 5.3: Schematic description of MTF measurement of a fiber amplifier.

5.3 Results

The modulation transfer functions of both the Yb-doped fiber laser and Er-doped fiber laser can be seen in Figure 5.4. The generalized Lorentzian function fit is applied to the graphs. The measurement is repeated for different modulation depths to make sure that the responsivity of the system is linear to the modulations. As seen from the graphs, the modulation of the pump power can be transferred to the laser power up to some frequency. Beyond that point, the modulations are suppressed by the laser. The reason of this suppression is the gain dynamics. The upper state lifetime of the gain medium limits the speed of the events, so that the gain can transfer from the pump signal to the laser signal. Once the gain is saturated by pumping it starts to be unresponsive to the change in the pump power before emitting light and being ready for inversion again. The faster modulations are suppressed by the gain medium. The MTFs are essentially flat up to a 3 dB cut-off frequency of around 80 kHz for the YDFL and around 15 kHz for the EDFL. The lower cut-off frequency is to be expected for Er-fiber, as the gain lifetime is longer than Yb-fibers by about the same amount. Thus the noise in the frequencies higher than the cut-off frequency does not couple from

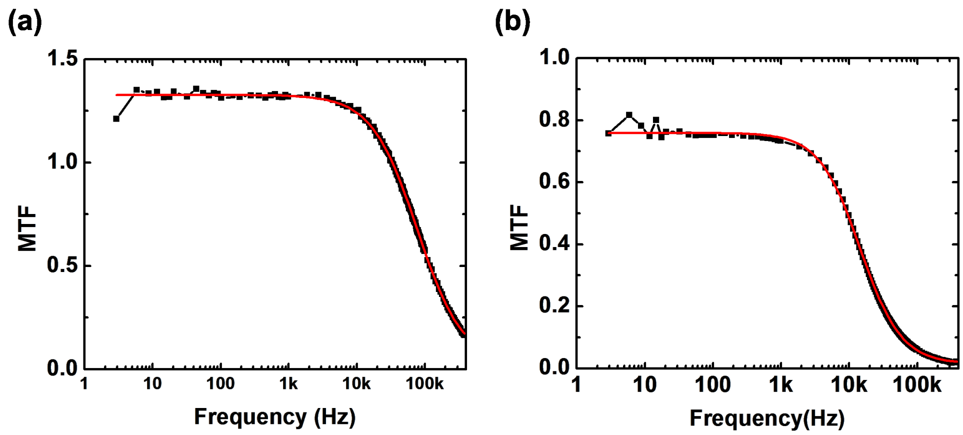

Figure 5.4: Modulation transfer functions of (a) Yb-doped fiber laser (b) Er-doped fiber laser.

the pump source. We can say that amplified spontaneous emission is responsible for laser noise at high frequencies. The cut-off frequencies also define the cut-off bandwidth of modulations that are intentionally applied to the pump power for stabilization.

In chapter 3 it is shown that the integrated laser noise depends on the cavity gain factor. It is examined also for noise transfer function, and seen that the plateau (flat region before cut-off) of the MTF depends on the cavity gain factor and increases with gain (Figure 5.5 (a)). It is an obvious result that if there is no gain, the fluctuations of pump power are not expected to affect the output signal. On the other hand, the more gain, the more effect of the pump power to the signal.

Once the modulation transfer function from the pump source to the laser is known, it is possible to estimate the absolute noise coupled from the pump laser to the laser by the simple calculation:

$$RIN_{\text{predicted}}\left(f\right) = MTF\left(f\right) \times RIN_{\text{laser}}\left(f\right). \tag{5.3}$$

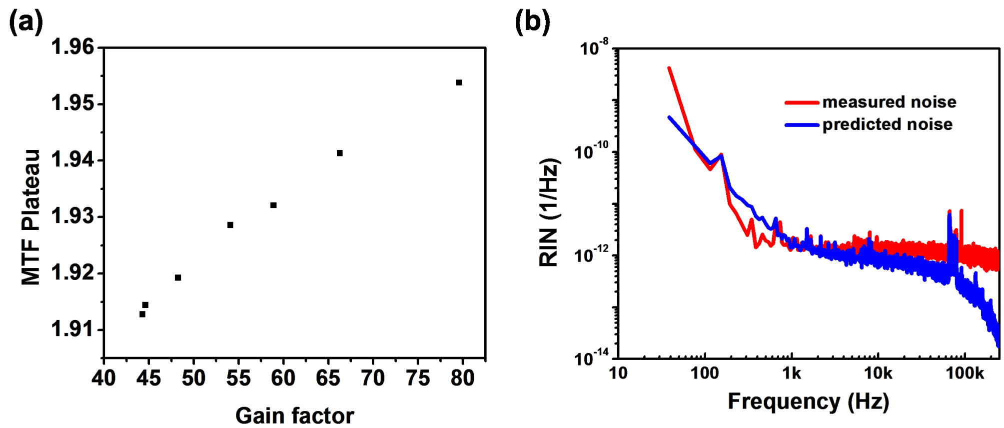

Figure 5.5: (a) MTF plateau value with respect to cavity gain factor (b) Predicted RIN by using MTF and pump diode noise.

The predicted laser noise is shown in the Figure 5.5 (b). The prediction is more accurate for the low frequencies, and it supplies a lower limit for the relative intensity noise of the laser.

In Figure 5.6 the modulation transfer function of Yb-doped fiber amplifier is given. The generalized Lorentzian funciton applies to the graphs. The black curve represents the transfer function from the pump source to the laser, and the red curve represents the transfer function from the seed source to the laser. The modulation transfer function of pump source is similar to the laser MTF, but MTF of seed source behaves in the opposite manner with respect to modulation frequency. For high frequencies the reasoning is similar. Gain dynamics are unresponsive to any event faster than its natural time scale. Otherwise, it would be impossible to amplify short pulses. For low frequencies, the same principle is applied in the opposite direction. Thus the modulations on the seed signal for frequencies lower than the cut-off frequency is suppressed by the gain medium. Furthermore, the results show that the amplifier's 3-dB cut-off frequency of MTF from the pump is lower than the laser's cut-off frequency. This can be as a result of the oscillatory nature of the lasers. The coupled dynamics of the signal power and gain is the main difference of the laser from the amplifier. As the relaxation

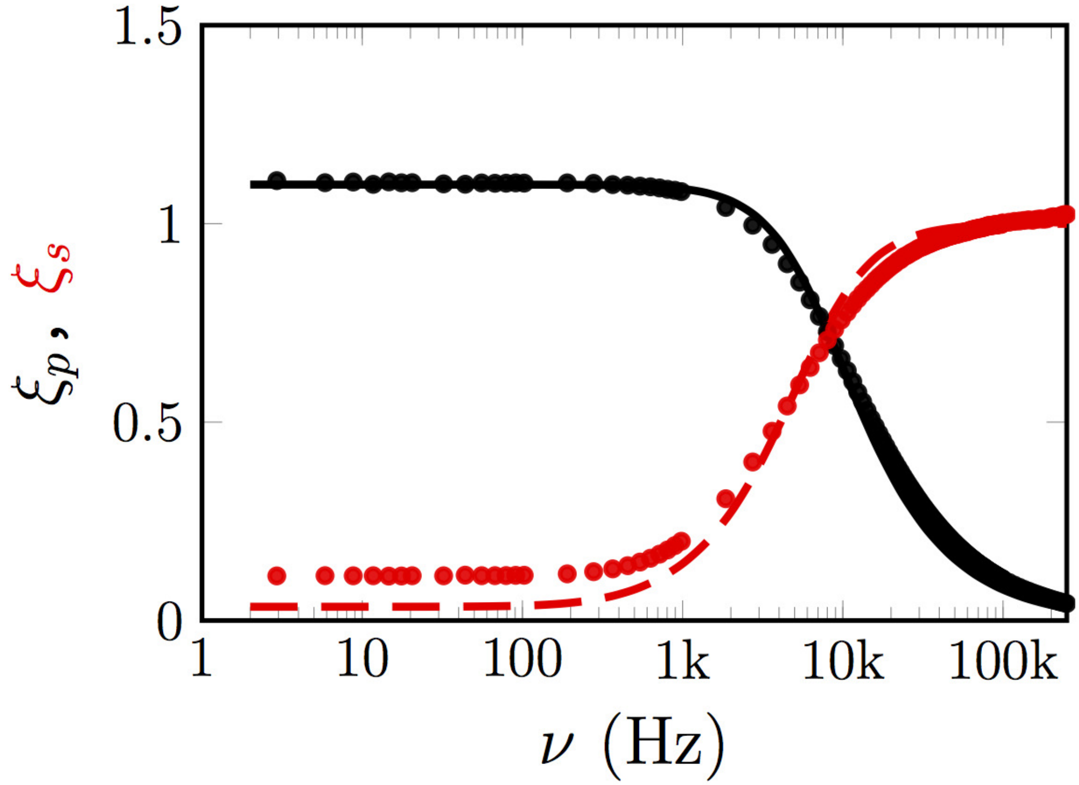

Figure 5.6: MTF for pump (black) and seed (red) signals of fiber amplifier.

oscillation frequency is in the order of a few 10 kHz, which is depended on the loss of the cavity and saturation energy of the gain, the cut-off frequency may shift to higher frequencies due to the resonance of the gain dynamics.

Since modulation transfer functions from the pump source to the laser and from the seed source to the laser are known it is possible to estimate the absolute noise of the amplifier by the following simple calculation:

$$RIN_{\text{predicted}}(f) = \eta_1 \left[RIN_{\text{s}}(f) \times MTF_{\text{s}}(f) + RIN_{\text{p}}(f) \times MTF_{\text{p}}(f)\right] + \eta_2 \left[RIN_{\text{ase}}(f) + RIN_{\text{p}}(f) \times MTF_{\text{ase}}(f)\right]. \quad (5.4)$$

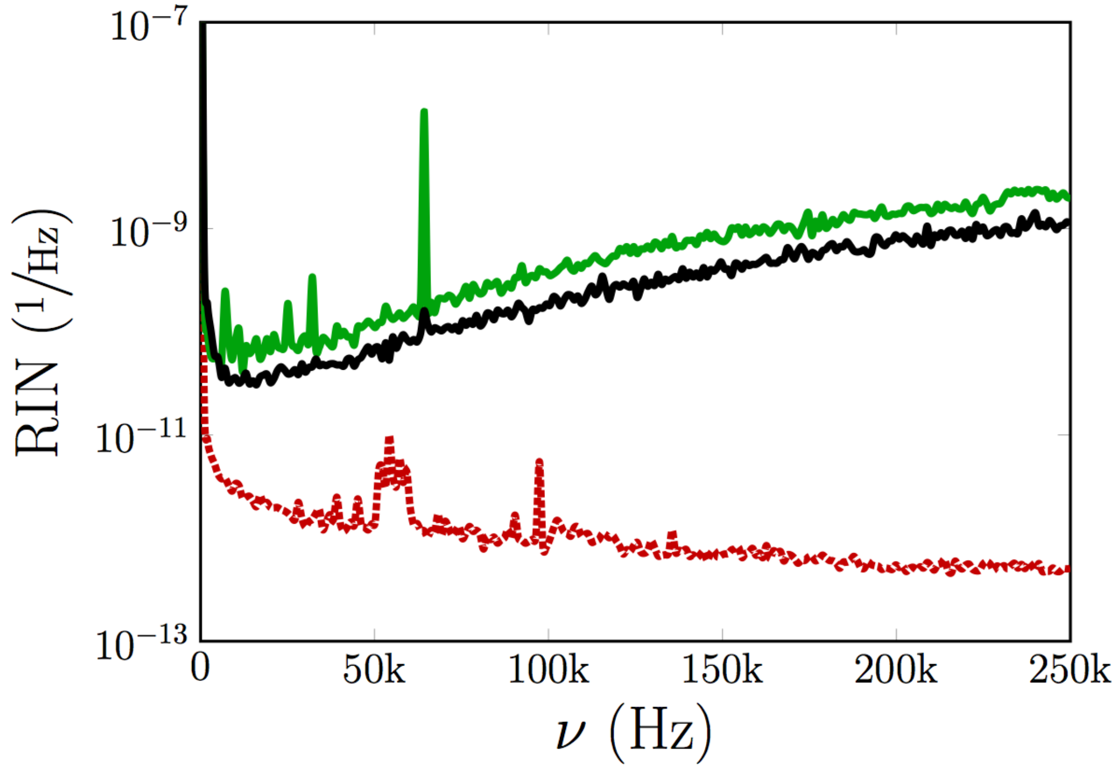

Figure 5.7: Predicted RIN of fiber amplifier (measured RIN (green), predicted RIN (black), RIN of seed (red)).

Here, η_1 and η_1 is the fractional power of the signal and amplified spontaneous emission (ase) portions of the amplifier output, respectively. $MTF_{\ ase}$ is the measured transfer function from pump-to-ASE, which has the same form as $MTF_{\ p}$. $RIN_{\ s}$ and $RIN_{\ p}$ represent the spectral noise density of the seed and pump signals. The relative intensity noise contributed by ase can be calculated with the optical bandwidth ($\Delta\upsilon$) of the ase as follows:

$$RIN_{\text{ase}}(f) = \Delta\upsilon^{-1}. \tag{5.5}$$

By adding all the contributions the amplifier noise can be predicted. Figure 5.7 shows the RIN of measured seed (red), and double-cladding amplifier output (green) and calculated amplifier output (black) at 1.5 W of seed and 72 W of pump powers. The integrated RIN values are measured and calculated to be 1.42% and 2.00%, respectively.

5.4 Conclusion

In conclusion, a systematic characterization of the coupling of modulations in pump power to the fiber laser is reported for Yb-doped fiber laser, and Er-doped fiber laser and Yb-doped fiber amplifier. The MTFs are essentially flat up to a 3 dB cut-off frequency of around 80 kHz for the YDFL and around 15 kHz for the EDFL. The cut-off frequencies also designate the modulation bandwidth of the fiber lasers by using the pump sources. In order to increase the bandwidth, both the seed signal and pump signal should be modulated at high and low frequencies respectively in the amplifiers. The obtained MTFs are used to predict the RIN of fiber lasers and amplifiers. The results supply a lower limit estimate of the noise level of the systems.

Chapter 6

Application of a Mode-locked Fiber Laser for Highly Time Resolved Broadband Absorption Spectroscopy and Laser-assisted Breakdown on Micro-plasmas

6.1 Introduction

The characterization results of the relative intensity noise of fiber lasers and amplifiers are summarized, and the methods to build a low noise fiber laser system are discussed in the previous parts of the thesis. In the following parts, some of the applications of low-noise laser systems will be reported, and the performance will be discussed. In this chapter, we demonstrate the possibility for pump-probe experiments by initiating plasma breakdown on a picosecond time scale (”pump”) with a high power beam, and measuring the broadband absorption with the simultaneously provided low-noise broadband signal (”probe”) where both the pump signal and probe signal are produced by the same fiber laser system. Since

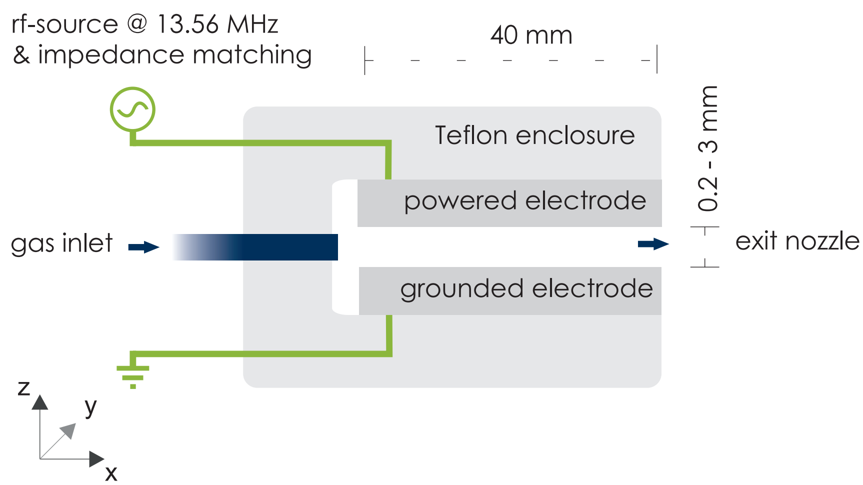

Figure 6.1: Scheme of the micro-plasma jet discharge.

both pulses are generated from the same mode-locked master oscillator, they have a strong level of synchronization limited by the timing jitter of the seed laser. The signal-to-noise ratio of the absorption spectroscopy is limited by the relative intensity noise of the probe signal. Furthermore, minimum detectable absorption also depends on the intensity noise level. Since the absorbances are usually small (in the order of 10^{-3}), a systematic study is required to operate the fiber laser system with low intensity noise. The fiber laser system is built by the author with the help of Kutan Gürel in Bilkent University, and the micro-plasma jet is prepared by Benedikt Niermann in the Ruhr-University Bochum. The experiments are carried out by Benedikt Niermann and the author in Ruhr-University Bochum. The results are published in Journal of Physics D [35].

The atmospheric pressure micro-plasma jet is a capacitively coupled, non-thermal glow-discharge at high pressures. The design concept of this discharge is based on the plasma jet introduced by Selwyn co-workers in 1998 [36] and advanced by Schulz-von der Gathen et al [37]. Feed gas flows between two closely spaced stainless steel electrodes driven at 13.56 MHz radio-frequency in a parallel plate configuration (Figure 6.1). Electrodes and plasma volume are enclosed by quartz windows, giving direct optical access to the discharge. The jet is operated in helium at various flow rates from 200 sccm to 5 slm. The electric field between the electrodes causes a breakdown in the gas and produces a plasma with electron temperatures and densities of about 1 to 2 eV and $10^{10} cm^{-3}$, respectively [38, 39]. Atoms and molecules in the feed gas become excited, dissociated or ionized by electron impacts. Since the electrons are not in thermal equilibrium with the ions and neutrals, the gas temperature remains a few tens of K above room temperature [40]. The distance between the two windows is fixed to 1 mm while the electrode gap size can be varied between 0.2 and 3 mm. In all presented configurations the discharge operates as a typical α-mode rf glow discharge.

Measuring the optical absorption of plasma species is a powerful method to deduce quantitative information on the (line-integrated) species density using the Lambert-Beer law. The most frequently used techniques are broadband absorption spectroscopy (BBAS) [41], tunable diode laser absorption spectroscopy (TDLAS) [42, 43, 44] and cavity ring-down spectroscopy (CRDS) [41, 45, 46]. The advantage of BBAS over TDLAS is the coverage of a large spectral range, facilitating the simultaneous measurement of several species in a plasma absorbing at different wavelengths. Its disadvantage compared with TDLAS is its lower spectral resolution. On the other hand, essentially for each optical transition a separate diode laser has to be employed for TDLAS. The advantage of CRDS is its very high sensitivity, provided that a long absorption length between two mirrors of very high reflectivity can be realized. In this technique, the characteristic decay time of the intensity of a light pulse is measured, which is coupled into the cavity with the species of interest. Due to the very small plasma volume, CRDS is difficult to realize if spatial resolution is required [47, 46]. Both TDLAS and BBAS have been successfully applied to micro-plasmas [48, 49, 50, 51, 52, 53]. Absorbances are usually small, rarely exceeding 10^{-3}, requiring in both cases a very stable setup. Often the lock-in techniques or other refined optical techniques are used to increase sensitivity. Since in low-pressure plasmas the width of the absorption lines is in the order of a few GHz, a very high resolution spectrometer has been required for BBAS. Whereas the line width of diode lasers in TDLAS is of the order of MHz and small compared with the absorption lines. This allows a precise measurement of the line profiles and may allow one to deduce, *e.g.*, the gas temperature or the electron density. In atmospheric pressure plasmas, the absorption lines are significantly broadened [51]. On the one hand, this reduces the signal-to-noise ratio further, but it alleviates, however, the line detection in BBAS. The highest signal-to-noise ratio is obtained when the spectral resolution of the spectrograph is identical to the line width [54]. For BBAS, several different light sources may be used such as, incandescent filaments, high-pressure Xe lamps or light-emitting diodes [53, 55, 54]. These light sources have to be well stabilized using precision power supplies and temperature control. They are normally not pulsed and spatially incoherent or at least highly multi-mode. Using a fast external chopper for lock-in techniques is important. Particularly interesting for the investigation of micro-plasmas is the use of supercontinuum radiation [56] generated from coupling very short pulse lasers into a photonic crystal fiber (PCF) [57]. Since this process produces pulses which are still in the picosecond range, typically with sub-picosecond timing jitter values, the use of the supercontinuum pulses allows superb time resolution of the measurement.

It is well-known that high intensities of laser radiation may induce a breakdown in gases and at surfaces, together with the formation of a plasma [58, 59, 60, 61, 62, 63]. Several studies on gas breakdown and surface-assisted breakdown has been published, and threshold values for breakdown have been communicated [60]. However, the data show a large scatter. It appears that several mechanisms may be invoked: very large electric field strength at high local laser powers, and secondary electron emission from the surfaces at low enough wavelength and/or material ablation/heating with subsequent charge carrier emission. These mechanisms may act simultaneously. It is usually observed that threshold values for gas breakdown increase for a given system with the wavelength of the laser light [60]. Laser irradiation of surfaces has been employed successfully to localize and clock the formation of short-pulse plasmas in corona-streamer discharges [64]. It is not possible to make a significancy order among the relevant quantities, namely, instantaneous intensity, power, pulse energy and fluence play a dominant role in setting the threshold level and thereby, the optimum experimental conditions. It is likely that several of these factors plays a role, thus leading to two separate thresholds, one for peak intensity and one for total energy. It is interesting to note that mechanisms similar to those of laser-surface interaction probably play a role in the glow-to- arc-transition as well.

To the best of our knowledge, there are no reports on "pump-probe" experiments using a single laser, nor two tightly synchronized lasers, generating a pump and a probe pulse for the establishment of a special state and its subsequent diagnostics, respectively, in the field of micro-plasmas. The evolution of an event can be monitored over several pulses using a variable delay between excitation and read-out pulse. This approach is an adaptation of the well-known ultrafast spectroscopy, notably in the laser-surface interaction at extreme laser powers [61]. It has yielded a wealth of most interesting physics information for transient phenomena. In our case, a custom designed fiber laser system is a unique and new approach to realize laser-assisted pump-probe experiments in micro-plasmas.

Supercontinuum generation is a process where laser light is converted to light with a very broad spectral bandwidth [65, 66]. When optical pulses propagate through a highly nonlinear medium their spectral evolution is affected by nonlinear effects like self phase modulation, cross phase modulation, four wave mixing, Raman scattering together with the dispersive properties of the medium. All of these nonlinear processes are capable of generating new frequencies and broadening the spectral width of the pulses extremely. The processes that contribute the supercontinuum generation depends on the temporal pulse width. For the picosecond regime, stimulated Raman scattering (SRS) and four wave mixing (FWM) are the most dominant processes in broadening the spectrum [66]. Since picosecond pulses are used to generate supercontinuum, we will only consider the responsible processes here.

FWM occurs due to the nonlinear response of bound electrons to an applied electromagnetic field. In chapter 2, the polarization induced in the medium is discussed (Equation 2.16):

$$\overrightarrow{P} = \epsilon_0(\chi^{(1)}\overrightarrow{E} + \chi^{(2)}\overrightarrow{E}^2 + \chi^{(3)}\overrightarrow{E}^3 + \ldots) = \overrightarrow{P}_{\text{linear}} + \overrightarrow{P}_{\text{nonlin.}} \tag{6.1}$$

FWM is a third order nonlinear process where $\chi^{(3)}$ is responsible. There are two types of FWM. The first one is the process where three photons are

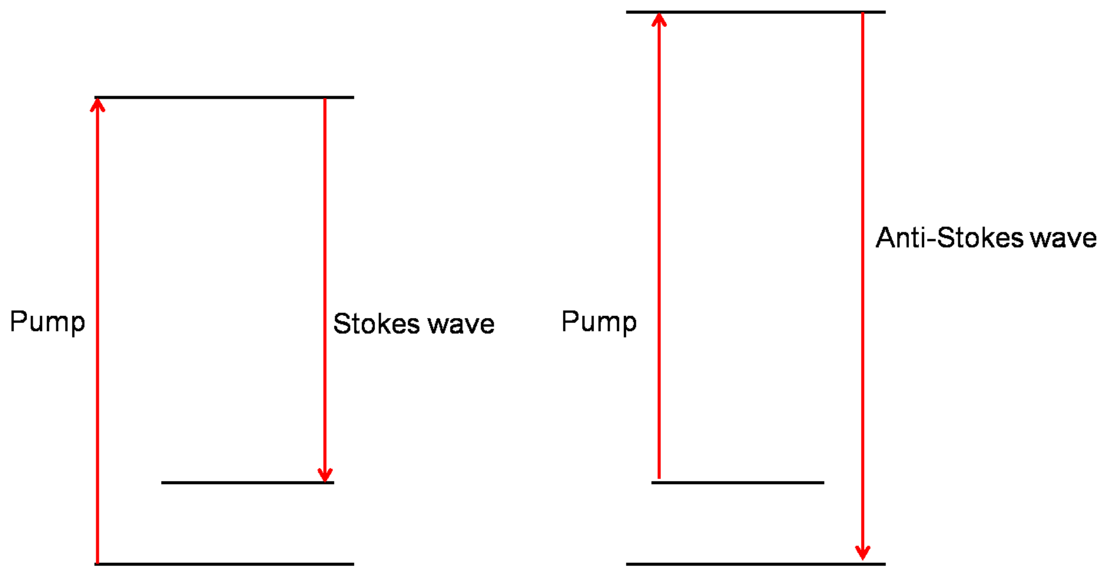

Figure 6.2: Raman scattering.

annihilated and a photon is created, which has energy equal to the total energy of seed photons.

$$\omega_4 = \omega_1 + \omega_2 + \omega_3 \tag{6.2}$$

This process is also responsible for third harmonic generation where $\omega_1 = \omega_2 = \omega_3$. Since the phase matching condition requires a critical arrangement, it does not occur in optical fibers with high efficiencies. The second process is the case in which two photons at frequencies ω_1 and ω_2 are annihilated, while two photons at frequencies ω_{13} and ω_1 are created simultaneously such that:

$$\omega_3 + \omega_4 = \omega_1 + \omega_2. \tag{6.3}$$

The phase matching is much easier in this process, since zero dispersion case supplies the condition.

SRS is also a third order nonlinear process where $\chi^{(3)}$ is responsible (Figure

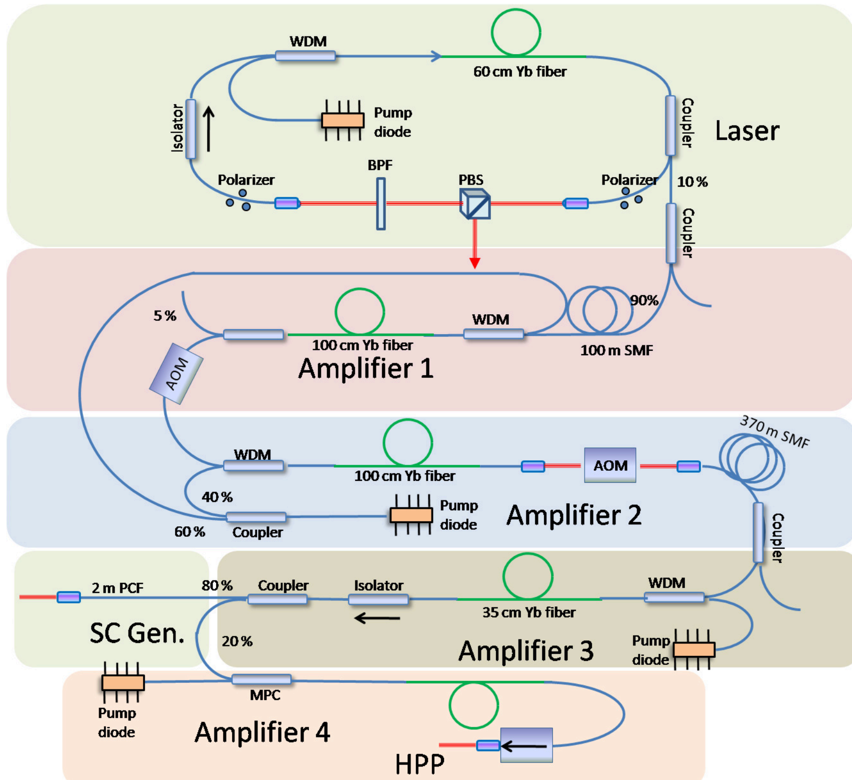

Figure 6.3: Fiber laser setup for supercontinuum and high-power pulse generation. WDM = wavelength-division multiplexing, PCF = photonic crystal fiber, MPC = multiport pump signal combiner.

6.2). It is a special case of Raman scattering in which, previously generated photons by Raman scattering, stimulate the other events and increase the Raman scattering rate. Raman scattering occurs due to the vibrational state transition of the molecules of the medium, after the interaction with the incident electromagnetic field. There are two possible Raman interactions. The first one is the Stokes Raman scattering where the emitted photon has a lower energy than the absorbed photon since the difference is absorbed by the vibrational modes of the medium ($\omega_s = \omega - \omega_v$). The second one is the anti-Stokes Raman scattering where the emitted photon has a higher energy than the absorbed photon, since the difference is given by the vibrational modes of the medium ($\omega_a = \omega + \omega_v$).

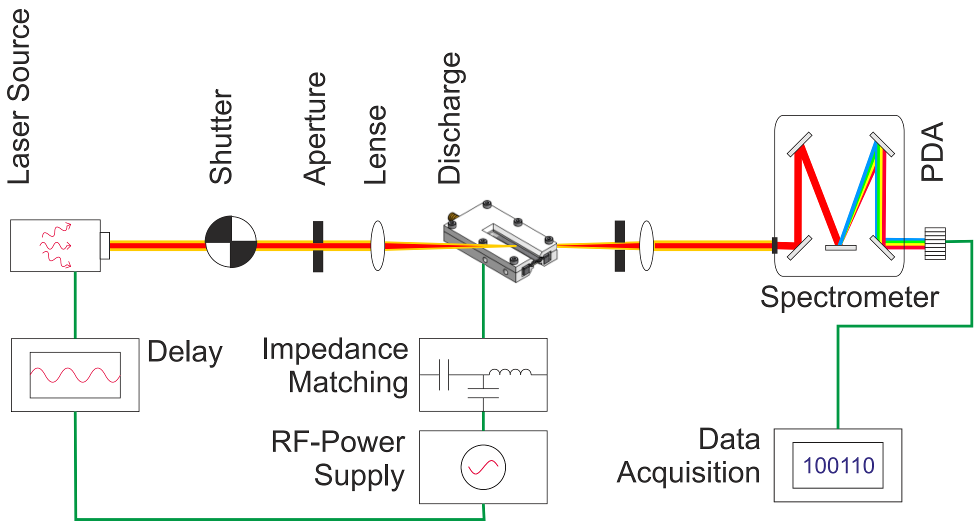

Figure 6.4: Experimental setup for broadband absorption measurements with supercontinuum source.

6.2 Experimental Setup

The fiber laser setup that was custom developed for this application is illustrated in Figure 6.3. The laser system comprises of a mode-locked fiber oscillator, operating in the all-normal dispersion mode, and seeding a multi-stage fiber amplifier. All-normal dispersion mode operation is preferred, since there is no need to use any diffraction grating pairs (diffraction grating pairs are normally being used to supply negative dispersion) which causes high losses to the cavity. For low noise operation, high losses are avoided. A multi-stage amplification is chosen to avoid high gain in a single amplification to decrease the amplified spontaneous emission ratio. A fiber stretcher is used to implement chirped-pulse amplification. The system is all-fiber, with an architecture based that of [67]. Prior to the final stage, the fiber path bifurcates into two, one seeding the power amplifier, which is described in detail by [23], and another seeding a highly nonlinear PCF for supercontinuum generation. Supercontinuum generation without pulse compression requires high pulse energies, so the repetition rate of the pulses is reduced to 50kHz in two steps to further increase the pulse energies during amplification, while maintaining reasonably low average power levels.

The oscillator comprises about 6 m of standard single-mode fiber for 1 μm wavelength (core diameter of 6.2 μm, NA of 0.14) and Yb-doped gain fiber (core diameter of 6.2 μm, NA of 0.14, $-500dB/m$ absorption at 976 nm). The length of the oscillator cavity defines the output pulse frequency of the laser in the mode-lock operation. The gain fiber is pumped in-core by a telecom-style 976 nm fiber-coupled laser diode with a maximum output power of 600 mW. Fast saturable absorption required for mode-locking is implemented via nonlinear polarization evolution. An output power of 14 mW at 27.12 MHz repetition frequency (set to exactly the second harmonic of 13.56 MHz) is obtained through a 10% output coupler after the gain fiber. The power of the seed laser is sufficient to suppress amplified spontaneous emission (ASE) generation in the subsequent amplifying stages.

Following another fiber coupler, around 90% of the output power from the oscillator traverses 500 m of single-mode fiber to stretch the pulses. The stretching is necessary to reduce the peak power of the pulses, and thus to minimize the nonlinear effects imposed on the pulses in the following stages. The remaining 10% of the beam is used for diagnostics.

The stretched pulses are amplified and then reduced in repetition rate through acousto-optic modulators (AOMs) to achieve the desired pulse energy in two steps. Amplifier stages consist of 1 m long Yb-doped fiber (of the same type as in the oscillator). 5% of the second AOM output is split off for diagnostics, and the rest seeds the third amplifier with 35 cm of Yb-doped fiber. The beam is split where 20% is used to seed the power amplifier and 80% is coupled into the 2 m of PCF for supercontinuum generation. We used a 976 nm diode with 8 W of maximum power for the power amplifier. The average output power of the power amplifier is around 1.1 W, obtained at pump power of 6 W, limited by the onset of nonlinear effects. At a final repetition frequency of 50 kHz, this corresponds to 22 μJ, which is among the highest obtained from a picosecond fiber amplifier. The pulse length of the supercontinuum pulses is about 300 ps with about 166 nJ pulse energy and an average beam power of 8.3 mW.

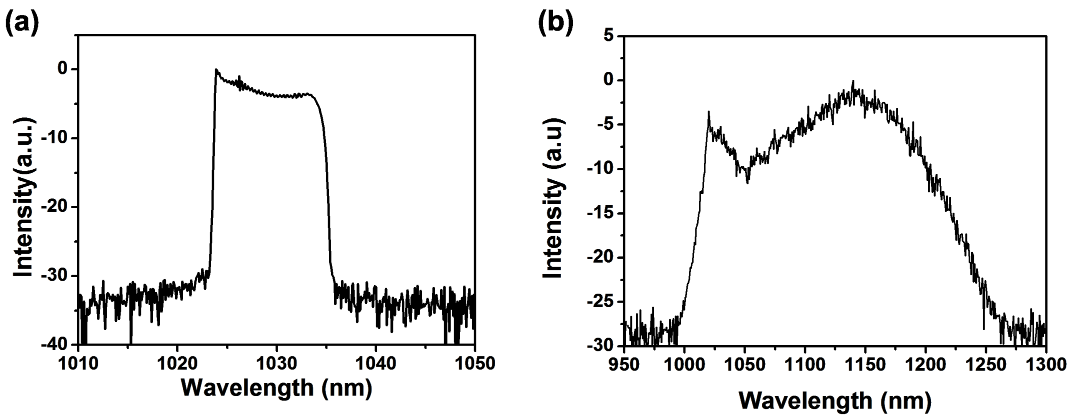

Figure 6.5: Optical spectra of the (a) laser output (b) high power amplifier output.

The experimental setup for BBAS measurements is shown in Figure 6.4. The supercontinuum beam from the fiber laser is focused into the discharge, where some portion of the beam is absorbed by diverse plasma species that offer transitions in the range of the supercontinuum spectrum. The transmitted beam is guided on the entrance slit of a spectrometer with 75 cm focal length, which is equipped with a 1200 lines mm^{-1} grating and images the signal to an InGaAs photo diode array. The effective resolution of the system is less than 50 pm. Due to the high spectral intensity of the supercontinuum, the slit opening can be as small as a few μm.

6.3 Results

There are two main requirements for the output of the fiber laser system: high energy pulses for pumping and low-noise broadband pulses for probing. The system provides these requirements in two separate arms seeded by the same mode-locked fiber laser. The seed laser is mode-locked in all-normal dispersion regime for low-noise operation and compact design. The integrated relative intensity noise of the seed laser is lower than 0.03%. The spectral output of the

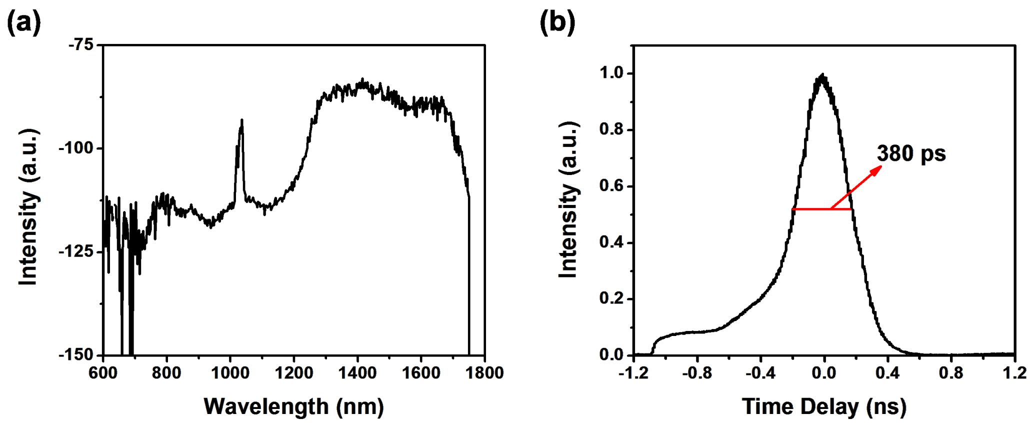

Figure 6.6: (a) Optical spectrum of the supercontinuum (b) Temporal shape of the high power output.

laser is typical for all-normal dispersion lasers (Figure 6.5 (a)). The spectrum of the optical signal does not change significantly until the second amplifier. In the second amplifier, the bandwidth increases from 12 nm to 15 nm, and in the third amplifier it rises up to 35 nm due to the nonlinear spectral broadening. The structures on the top of the spectrum of the high power output (Figure 6.5 (b)) are due to the nonlinear effects. Although the average power of the optical signal does not change dramatically, pulse energy and peak power of the pulses increase since the repetition frequency of the pulse train decreases. At the output of the third amplifier stage, the system produces 1.2μJ pulses at 50 kHz repetition frequency.

The fiber laser system's first output is the supercontinuum, which is seeded by the output of the third amplifier. 1.2μJ pulses are enough to generate a broadband spectrum (Figure 6.6 (a)). The emission spectrum of the system ranges from roughly 700 to 1700 nm, with an intensity profile ranging over about three orders of magnitude. The integrated RIN is lower than 0.25% (Figure 6.7 (a)). The system's second output is the high energy pulses extracted from the high power amplifier port. 22 μJ pulses are produced at the repetition frequency of 50 kHz. The pulse width is around 400 ps (Figure 6.6 (b)) and the peak power

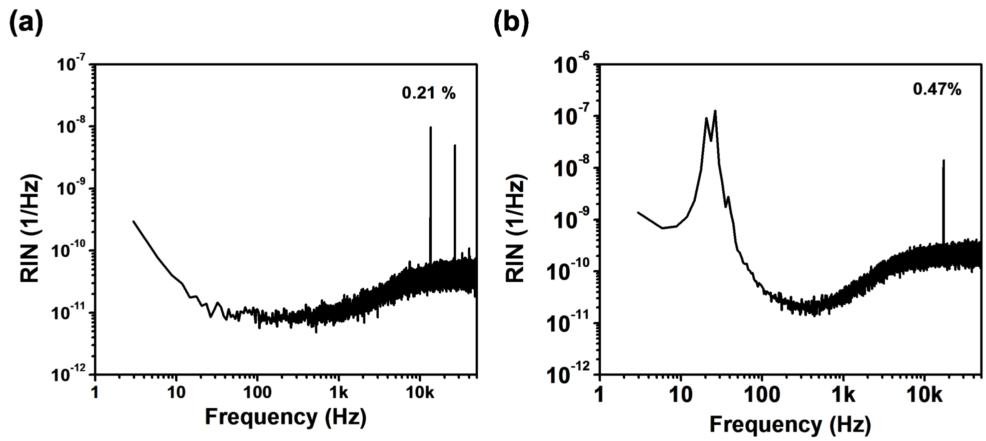

Figure 6.7: RIN of the (a) supercontinuum (b) high power output

is 55 kW. The spectral noise density of the pulse train is plotted (Figure 6.7 (b)) and the integrated RIN is calculated to be lower than 0.5%. The difference in integrated RIN, between supercontinuum and high power pulses, occur due to the high power pump source used in the final amplification stage.

A typical absorption spectrum around the He^m $2^3S_1 \rightarrow 2^3P_J^0 \quad (J = 0, 1, 2)$ transitions at 1083 nm is shown in Figure 6.8 (a) (black line). It was recorded with the spectrometer described above, in which the spectrum is already corrected for the instrumental broadening of the optical instruments and the entrance slit of the spectrometer. Also, three Voigt functions are displayed, representing the respective transitions from the He^m 2^3S_1 level. The functions have been modeled with the results obtained by TDLAS measurements which have been discussed in detail by Benedikt Niermann [68]. Although the spectral resolution of BBAS is limited, compared with the possibilities of tunable diode lasers, these results show that sufficient information can be extracted to retrace the line profile and obtain a perfect agreement with TDLAS measurements.

The detection limit of BBAS using supercontinuum radiation on the given discharge geometry is at least in the order of 10^{-3} as shown by Figure 6.8 (b),

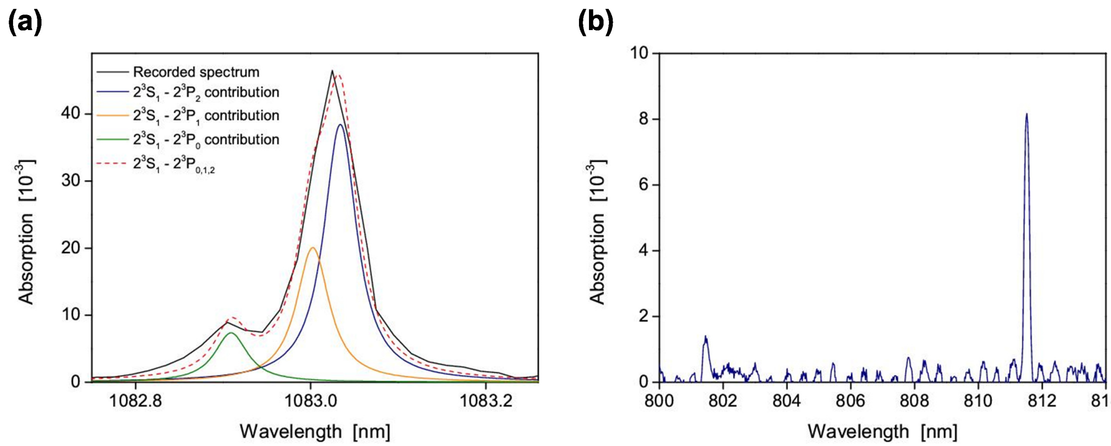

Figure 6.8: (a) Absorption spectrum around the He^m $2^3S_1 \rightarrow 2^3P_J^0 \quad (J = 0, 1, 2)$ transitions at 1083 nm (black line). Recorded with a spectrometer featuring 75 cm focal length, 1200 lines per mm grating and few m slit openings, together with a photo diode array as a detector. (b) Absorption spectrum around the argon transitions at 801.5 and 811.5 nm.

which presents two argon transitions at 801.5 and 811.5nm. The sensitivity depends critically on the extend of the periodic noise pattern visible in this graph. This noise pattern is the consequence of an etalon effect, between the glass plates that confine the discharge channel of the micro-plasma jet. These limitations can be suppressed by operating the jet discharge without the glass windows in an airtight chamber filled with the working gas, extending the detection limit further.

After showing the effectiveness of BBAS for the application on micro-plasma, the investigation of transient phenomena requires a well-synchronized connection to the trigger that transfers the plasma into another mode. The RF voltage thresholds for plasma ignition and collapse in the micro-plasma do not overlap, but show a certain hysteresis, where the discharge ignites at higher voltages than it collapses when decreasing the electrode voltage. This hysteresis effect is visualized in Figure 6.9. The hysteresis length depends on a variety of factors, such as the electrode gap width, the gas mixture as well as the electrical characteristics of the matching network, but it can account for up to 25% of the overall voltage.

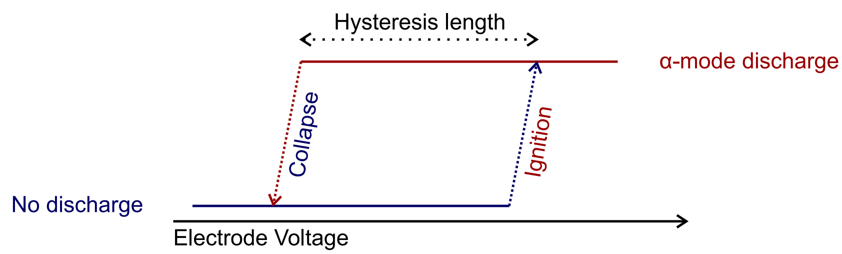

Figure 6.9: Discharge ignition and collapse hysteresis of the micro-plasma jet.

The plasma is successfully ignited with high energy pulses of the fiber laser system. Once the discharge is ignited, the plasma remains in a stable α-mode as long as the electrode voltage is above the collapse threshold. One application of this external plasma ignition is the opportunity of highly time-resolved diagnostics of the ignition phase. Usually the rise of excited species after the ignition is slightly affected by the rising power level of the RF generator. With the help of the high-power laser beam, it is possible to activate the RF generator below the ignition threshold and activate the discharge once the RF power is stable. Furthermore, since the RF phase can be synchronized with the laser frequency, the laser is able to set the ignition point with a precision of less than 100 ps and at a selectable phase of the RF cycle.

6.4 Conclusion

In conclusion a high energy fiber laser setup is constructed for studies on micro-plasma jets. The system produces 22 μJ pulses at 50 kHz from one arm and broadband pulses (around 700 nm at 30 dB) from the other arm. The energy level is one of the highest obtained from a picosenond fiber laser system. The integrated noise level of broadband signal is around 10^{-3}. The high energy pulses succeed to ignite the micro-plasma jet in which helium gas flows and driven with 13.56 MHz ac signal. Furthermore, BBAS measurements using a fiber laser generated supercontinuum spectra provide a way for absorption spectroscopic measurement over a broad spectral range with detection thresholds down to 10^{-4}

in the absorption signal. The hysteresis of discharge ignition and collapse together with the possibility of phase-locked laser-assisted breakdown, offers a tool for highly time-resolved studies of the plasma breakdown process.

Chapter 7

Development of Ranging and Sensing Technology with Fiber Laser Systems

7.1 Introduction

Ladar, which is the acronym of Laser Detection and Ranging, is a remote sensing device that measures the distance from a target illuminated with a laser. There is a wide area of applications for ladars like plotting topography [69], 3D imaging [70], meteorology [71, 72], military [73], geology [74], astronomy [75, 76], *etc...* There are two main parts of a ladar: transmitter and receiver (Figure 7.1). In this chapter fiber laser systems built as transmitter sources for ladar systems are described and the performances of the systems are discussed. Since the minimum detectable power and false alert ratio depend on the intensity noise of transmistter laser, the ladar is a convenient application to test the performance of low-noise fiber laser systems. The laser system in the first section is mostly built by Ebru Bayrı and Ihor Pavlov, the author attended for the optimization of the system for the ladar application. The laser system in the second section is built and optimized by the author and Ebru Bayrı.

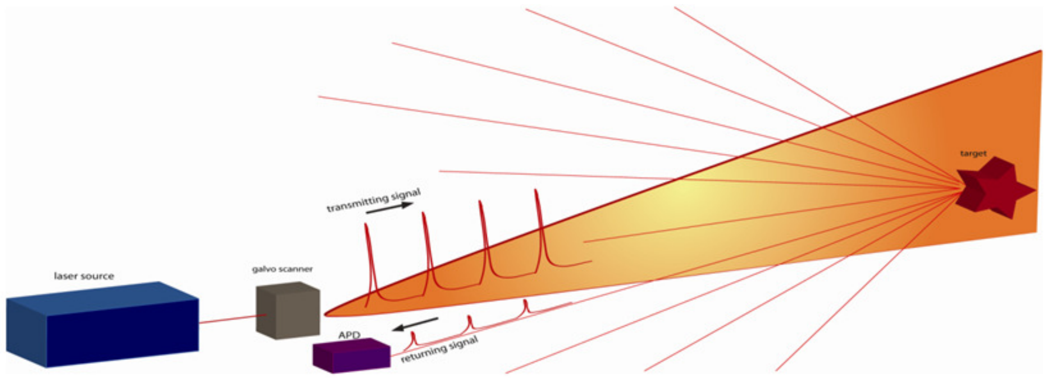

Figure 7.1: Schematic of a ladar.

Fiber laser has many advantages to be used as a transmitter source. All-fiber systems are alignment-free and it makes them stubborn against vibrations and various environmental conditions. Furthermore, due to the cylindrical geometry of fibers, heat dissipation is faster and system can handle higher power levels without active cooling. Plug-in efficiency of fiber laser systems is better than the other system (around 3% for the total ladar system). They are more compact and more importantly able to be shaped which makes them more friendly for compact packaging. Moreover, single-mode operation decreases the beam divergence of the ladar which increases the measurement resolution and maximum range of the ladar systems.

7.2 Fiber Laser System as a Transmitter of a Direct Detection Ladar

The working principle of a direct detection ladar is measuring the time of flight of a laser pulse transmitted from the system and reflected from the target (Figure 7.1). The critical parameters of a direct detection ladar are the maximum range, maximum unambiguous range and volume of the resolution cell.

The maximum range of a ladar system defines the maximum distance that a

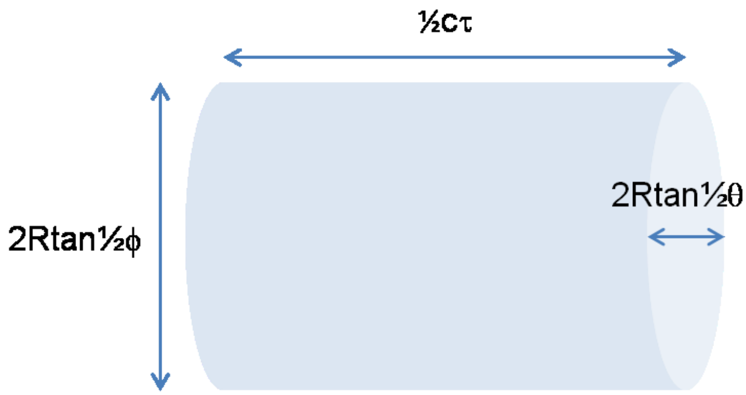

Figure 7.2: Resolution cell.

system can detect or range a target. The pulses reflected from the target and received by the detector should have power at least higher than the noise equivalent power (NEP) of the detector. Thus, the critical parameters are the NEP of the detector, maximum laser power, laser wavelength (atmospheric attenuation depends on wavelength), beam divergence of the transmitted pulse, acceptance angle and radius of the receiver optics. Hence, the main requirements for laser power, wavelength and beam divergence are determined by the maximum range capacity of the ladar.

The maximum unambiguous range of a ladar system defines the distance that a laser pulse can be reflected and received by the detector, before the next pulse is transmitted. It constrains the repetition frequency of the laser pulses where:

$$Maximum \quad unambiguous \quad range = \frac{c}{2 \times \omega_{\text{rep}}}. \tag{7.1}$$

A ladar system cannot distinguish two targets separately if they are in a single resolution cell. The range resolution is determined by the pulse width of the laser, while the lateral resolution is determined by the beam divergence (Figure 7.2). The volume of the resolution cell is also important to decrease the noise due to the volume clutter. Thus the pulse width is very important for the resolution and

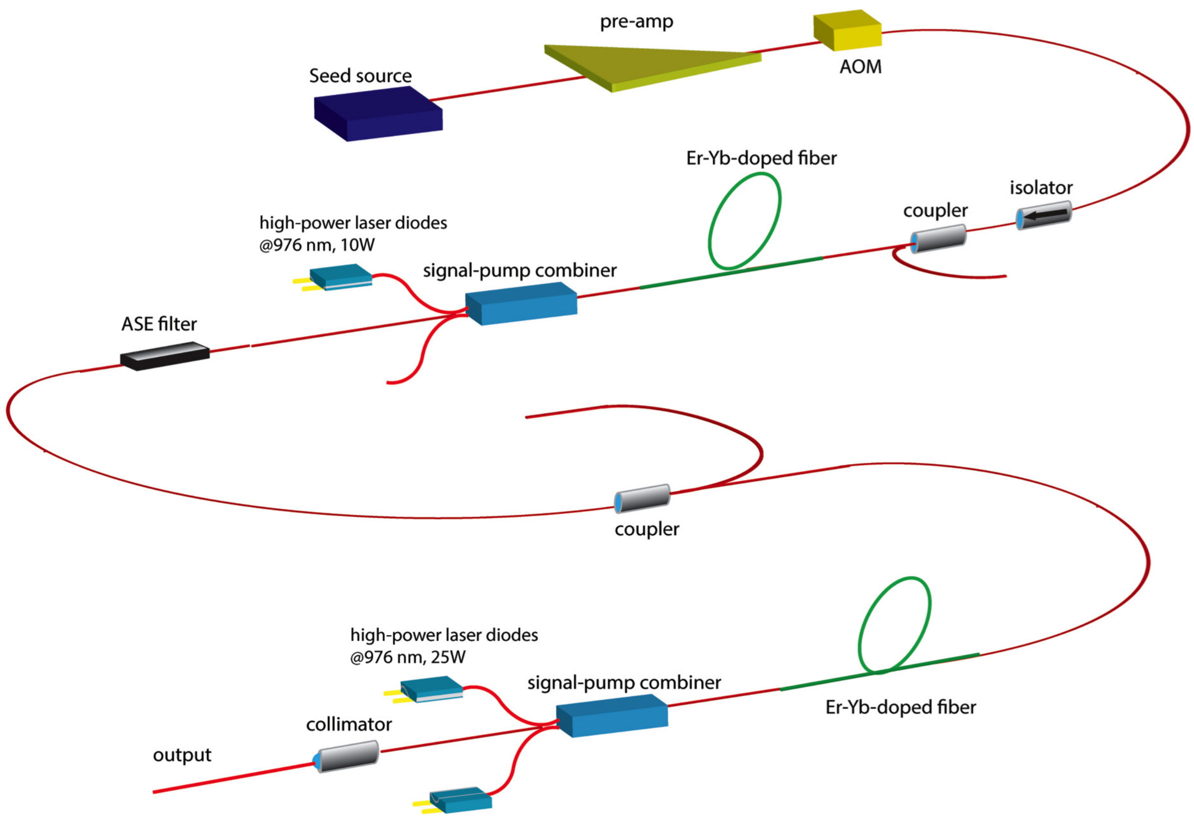

Figure 7.3: Schematic of the fiber laser setup.

noise of the ladar system.

To summarize, the requirements for a ladar system constrains the parameters of the laser built as a transmitter. For this purpose, a pulsed fiber laser system is constructed.

The schematic of a fiber laser system can be seen in Figure 7.3. A distributed feedback diode laser (DFB) is used as a seed source. A distributed feedback diode laser is a type of diode lasers where the emitting wavelength is selected with diffraction gratings [77]. The grating is constructed in order to reflect only a narrow band of wavelengths, and thus produces a single longitudinal lasing mode. In this laser a fiber Bragg grating is used for wavelength selection.The DFB laser is driven with a modulation at kHz level repetition rate and around 10 ns pulse

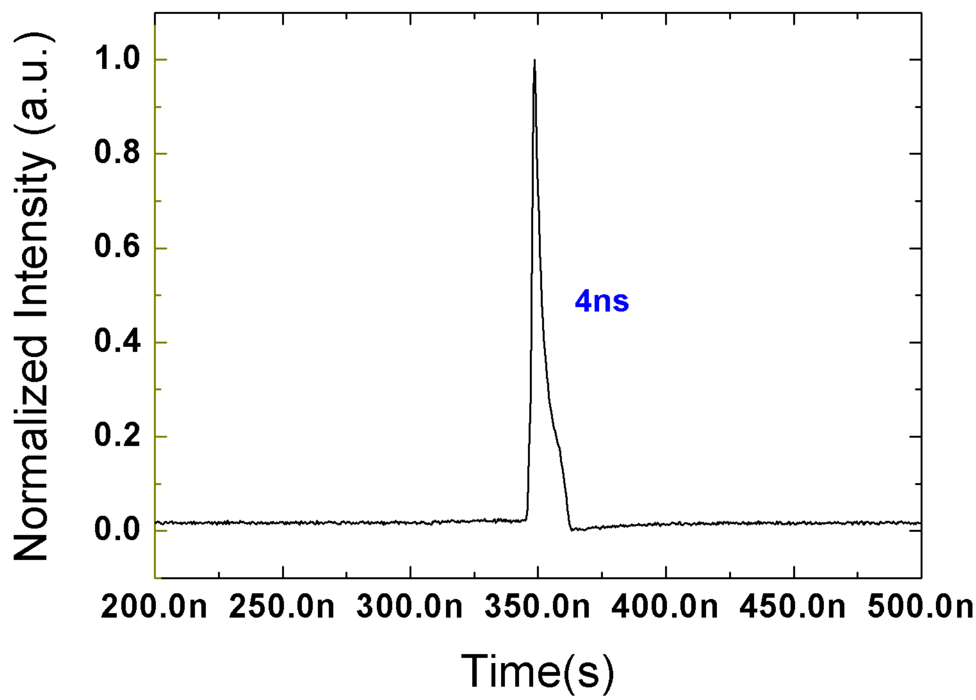

Figure 7.4: Temporal shape of pulses.

duration by using the electronic circuit developed in Meteksan Savunma. The central wavelength of the system is at 1550 nm which is in the eye-safe region and inside the infrared atmospheric window.

The fiber laser amplifier system consists of three Er-doped fiber amplification stages and one pulse picking stage between the first two amplifiers. The input and output power of the amplifier stages are optimized for decreasing the amplified spontaneous emission level in the ultimate pulse train, to increase the energy of a single pulse. The seed source produces 0.15 mW pulses with 10 ns pulse width at 500 kHz repetition rate. An acousto-optic modulator is used as the pulse picking stage to decrease the repetition frequency to 100 kHz. The DFB laser is driven at 500 kHz rather than 100 kHz to keep the average power at moderate levels, otherwise to amplify such low power will increase ASE and RIN of the signal as

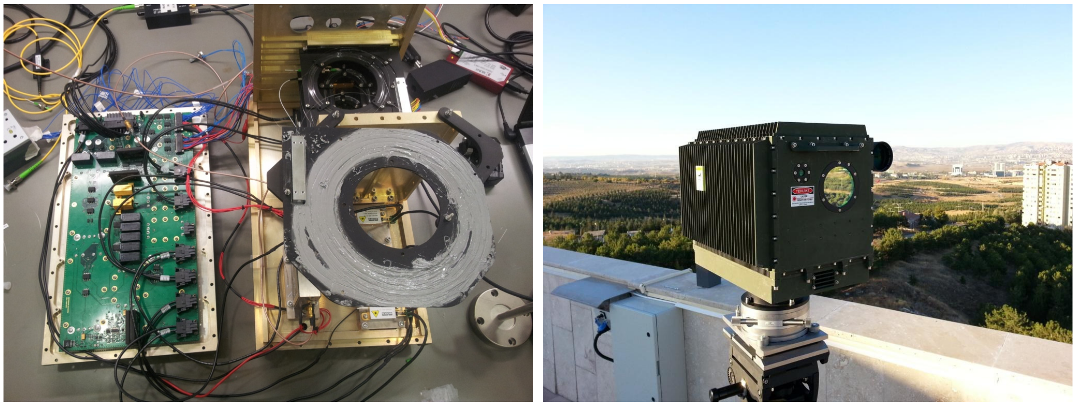

Figure 7.5: (a) Fiber laser system inside ladar. (b) Ladar.

discussed in the fourth chapter. The system produces 10 W average power with around 4 ns pulse duration at 100 kHz repetition rate, which means around 25 kW peak power (Figure 7.4). To the best of our knowledge, this system is the highest peak power ns single mode fiber laser system ever built.

Only the high power stage is necessary to be cooled as seen in Figure 7.5 (a). In this stage 30 W pump power is used and 10 W signal power is extracted. Thus, almost 20 W power is dissipated as heat on the fibers. The ladar system is qualified from the environmental tests (Figure 7.5 (b)). It can operate at the temperatures between $-20°$C and $50°$C and can be stored at the temperatures between $-30°$C and $60°$C. Furthermore, it can survive in the vibration of a Sikorsky helicopter without any change in the performance.

The maximum range of the ladar system is 1.5 km limited by the unambiguous range since the repetition frequency is 100 kHz. The beam divergence is smaller than 1 mrad since the pulses are extracted from single mode fiber. Hence 1 m lateral resolution is supplied in 1 km distance. The range resolution is smaller than 1 m since the pulse width is around 4 ns.

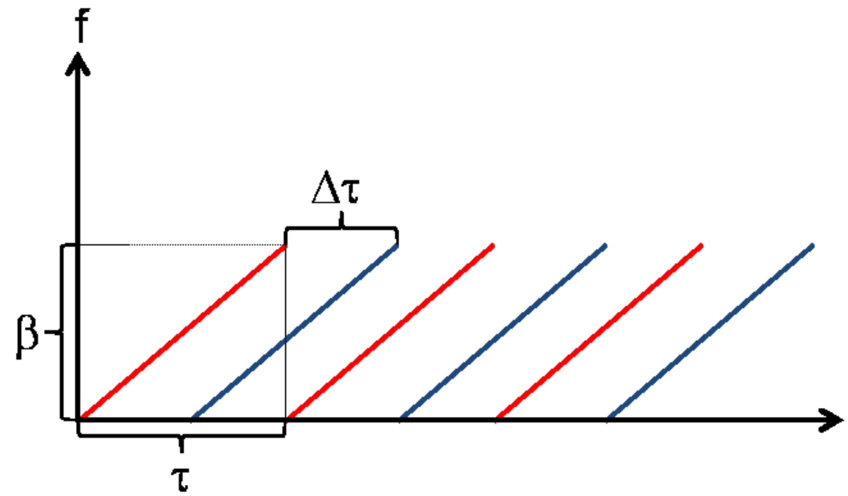

Figure 7.6: FMCW technique.

7.3 Fiber Laser System as a Transmitter of a Coherent Detection Ladar

The working principle of coherent detection ladar is beating the reflected signal from the target with a reference signal where both signals are generated by the same coherent source. In this application, frequency modulated continuous-wave (FMCW) technique is used to decrease the range resolution of the ladar (pulse compression technique for radars) [78]. The critical point in coherent detection is that, the coherence length of the source laser should be longer than the path difference of two signals. The main advantage beside direct detection is the ability of speed measurement of the Doppler effect.

In FMCW technique the frequency of the signal is modulated in time, hence there occurs a frequency difference between two signals due to different arrival times (Figure 7.6). Thus, the beat frequency of the two signals will be depended to the path difference.If the frequency is modulated linearly with time, like in the figure, the frequency difference will be as in the following:

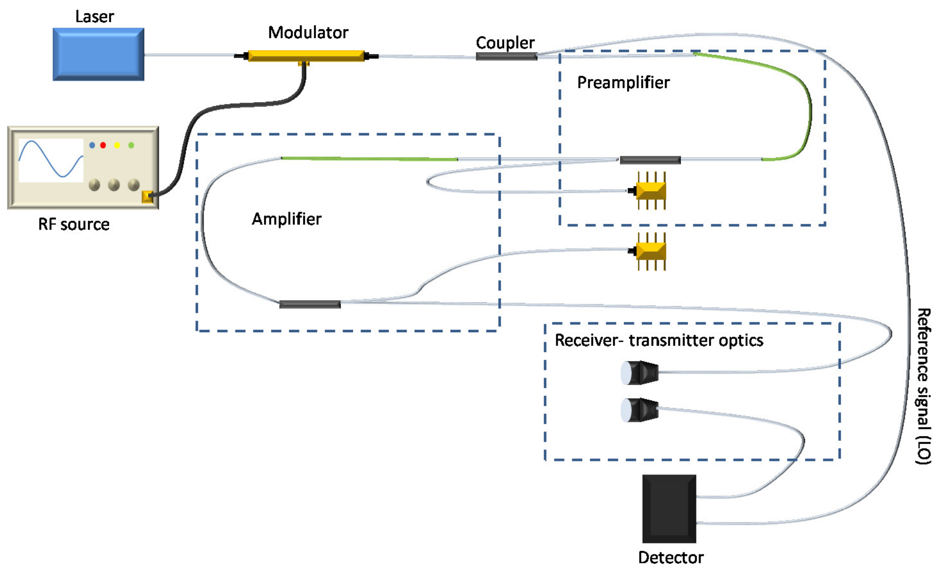

Figure 7.7: Schematic of the fiber laser setup.

$$f_{\text{beat}} = \frac{\beta}{\tau}\Delta t. \tag{7.2}$$

Here β is the modulation bandwidth, τ is the modulation period, Δt is the arrival time difference. As seen from the Figure 7.6 the frequency difference is constant, and the beat signal will be integrated during the period τ. In FMCW technique, the range resolution is determined by the reciprocal of the modulation bandwidth, and the unambiguous range is determined by the period τ.

As a transmitter laser of a FMCW ladar system, a fiber laser system is constructed (Figure 7.7, Figure 7.8). A semiconductor laser with 5 kHz bandwidth -which means 60 km coherence length- is used as the seed source. The laser wavelength is at 1550 nm, so Er-doped gain fiber is used in amplifier stages. The laser signal frequency is modulated by an electro-optic phase modulator to apply the FMCW technique, and the output of the modulator is divided into two arms to extract the reference signal. The other arm is amplified in Er-doped fiber amplifier stages from 50 mW to 10 W, in two steps. Two fiber coupled collimators are used as transmitter and receiver optics. The beam divergence is smaller than 0.3

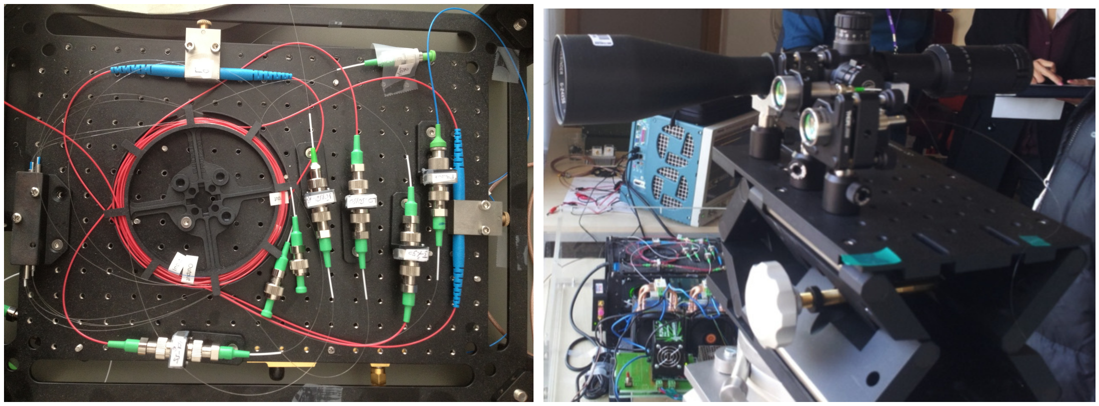

Figure 7.8: (a) Fiber laser system inside ladar. (b) Ladar.

mrad in the free space.

The frequency of the laser is modulated in 50 μs with a bandwidth of 75 MHz. Thus the range resolution of the FMCW ladar is 2 m and the maximum unambiguous range becomes 7.5 km.

7.4 Results

Both ladar systems are tested in the open air with realistic conditions in two days. An energy transfer wire with 1 cm radius is placed in around 1 km distance from the ladar systems as a target. The performances of two ladar systems are examined in the daylight with high visibility distance (higher than 10 km).

In the test setup, arranged for direct detection ladar, the distance between the ladar setup and target is measured as 1028 m, with a calibrated global positioning system receiver (GPS). The laser average power is measured as 10 W just after the transmitter collimator. The ladar is oriented to the wire with a boresighted binocular. It is observed that when the binocular is oriented to the wire, the ladar software detected an obstacle at 1028 nm. The measurement is controlled by observing the disappearing of the signal when the wire is removed. Furthermore, the ladar succeeds to resolve two wires, located 1 m apart.

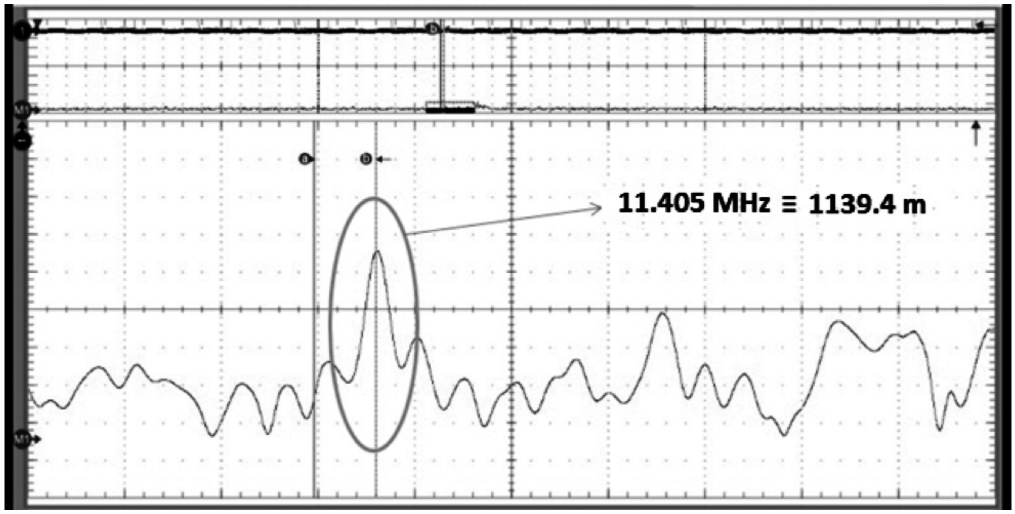

Figure 7.9: Ranging result with FMCW technique.

In the setup, arranged for the coherent detection ladar, the distance between the ladar setup and target is measured as 1139.4 m with the same GPS. The same procedure is repeated to orient the ladar to the wire, and the laser power is measured as 10 W. FMCW technique is applied by modulating the laser with 75 MHz bandwidth in 50 μs. It is observed that when the binocular is oriented to the wire, a peak arise at 11405 MHz in the Fast Fourier Transform trace (FFT) of a calibrated oscilloscope (Figure 7.9). The signal to noise ratio (SNR) of the measurement is monitored to be smaller than 10 dB. When equation 7.2 is used, the distance is calculated as 1139.4 m. The speed of light is taken as 2.997143×10^8 m/s for 1000 m altitude. The measurement is controlled by observing the disappearing of the signal when the wire is removed.

Finally the coherent detection ladar is also tested on a moving target. The laser directed on to a colleague standing 1039.4 m distant from the system. The beat signal is again observed on the oscilloscope (Figure 7.10 (a)). The beat frequency is shifted around 500 kHz due to the Doppler effect, when the colleague starts to walk toward the system (Figure 7.10 (b)). The velocity can be calculated as follows:

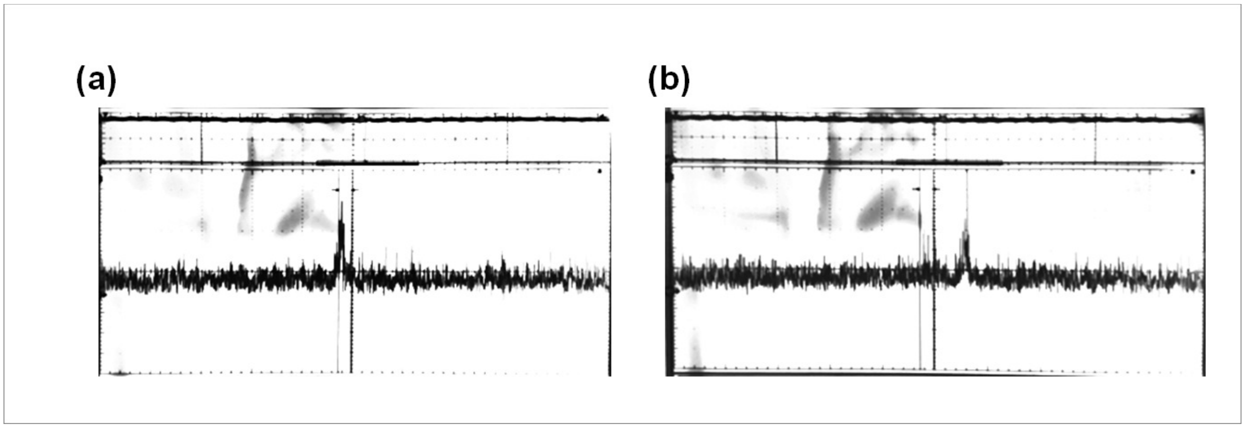

Figure 7.10: Ranging result with FMCW technique (a) for a stable target (b) for a moving target. The shift in the in beat frequency can be seen when the cursors are taken as reference points.

Detection method	P_{ave}	t_{meas}	D	θ	d	SNR
7 Direct detection	10 W	10 μs	72 mm	0.56 mrad	1128 m	$> 10dB$
Coherent detection	10 W	50 μs	15 mm	0.3 mrad	1139 m	$< 10dB$

Table 7.1: Comparison of the performances of direct detection and coherent detection ladars. P_{ave} is the average power of transmitter lasers, t_{meas} is the measurement time, D is the diameter of receiver optics, θ is beam divergence, d is the distance between the target and the system and SNR is the signal to noise ratio

$$v = \Delta f \times \lambda = 500kHz \times 1550nm = 0.77m/s = 2.8 \quad km/h. \tag{7.3}$$

In the Table 7.1 the measurement results of coherent detection are compared with the results of direct detection. If the values are carefully examined, the success of direct detection can be detected against coherent detection (around 10 times). In the coherence detection method, to increase the diameter of receiver optics, larger than the diameter of transmitter optics, does not improve the measurement performance, since the spatial fringes occur on the detector. Thus, direct detection is more convenient method for ranging applications, on the other hand the ability of measuring the speed of moving targets is the most important advantage of coherent detection.

7.5 Conclusion

In conclusion, a direct detection ladar system and a coherent detection ladar system have been constructed with fiber laser systems used as transmitter sources. The laser sources are custom built systems and optimized for the applications. To the best of our knowledge the fiber laser system for direct detection produces the highest energy picosecond pulses from a single-mode fiber system.

Both systems are presented as prototypes of a high resolution obstacle detection system for helicopters. They succeeded to detect a wire with 1 cm radius from 1 km distance with a resolution better than 2 m. Direct detection appears to be advantageous in ranging applications in terms of signal to noise ratio and power requirements. However, coherent detection is also able to give the velocity information of moving targets, and this capability renders it unrivaled for certain applications. It can be concluded that a hybrid system is the best option for ranging and motion detecting. This study concludes that fiber laser systems have tremendous performance as transmitter sources for ladars. They are inexpensive in terms of building and repairing costs and their modular architecture, make them easy to be serviced and repaired.

Chapter 8

Conclusion

In this thesis, studies on the relative intensity noise of fiber lasers and amplifiers and some examples of the applications of low-noise fiber laser systems have been presented. The results are enlightening a way to predict the noise of systems and build low-noise fiber lasers and amplifiers. Furthermore, the results provide important improvements for understanding the rich dynamics of the fiber laser systems.

A systematic characterization of intensity noise of mode-locked fiber lasers and amplifiers is reported. It is seen that noise does not depend sensitively on the mode-locking regime of the laser. Although there are rich dynamics in the evolution of the different mode-locking regimes, most of the events are fast processes like nonlinear response of the medium, to be distinguished in the spectral noise density of the laser, which is limited by the measurement bandwidth of 250 kHz. Only all-normal dispersion regime (ANDi) is observed to be slightly less noisy than the other mode-locking regimes. Other than the mode-locking dynamics, the only difference is the absence of the diffraction gratings in the architecture of the cavity of the ANDi laser. The high losses due to the low efficiency of the diffraction gratings cause an increase in the noise level of the other mode-locking regimes. In this direction, a systematic characterization of the intensity noise of the mode-locked fiber lasers with respect to cavity losses is reported. It is concluded that higher cavity finesse improves the noise performance of the laser.

In other words, maximizing energy extraction by increasing the output-coupling ratio has a detrimental effect on the noise performance. Thus, most high-energy lasers reported in the literature so far may have had a relatively poor noise performance. The extracted energy can also be increased by increasing the pump power of the laser. However, in this case the energy of pulses propagating through the cavity also increases, and causes different effects on the noise performance of the laser. It is observed that there is no change in the noise level up to threshold energy. Beyond the threshold level, nonlinearity-induced instabilities occur. The laser may start to form a continuous-wave signal extra to the pulses or multiple pulses inside the cavity. Although these effects are the main signatures of instable operation of the laser, they increase the intensity noise of the laser by less than 2 times. Since continuous-wave operation and multiple pulse formation are also natural behaviors of the laser dynamics, it is an expected result. However, unless these two instabilities are observed, the laser unexpectedly transitions to a high-noise state. The transition is abrupt and the noise difference is almost 100 times between the low-noise state and high-noise state. Thus, there is risk to produce higher noise laser pulses from a single laser than a high power laser system. Furthermore, it is hard to distinguish a laser operation at high-noise state from low-noise state by observing the spectrum and autocorrelation traces of the pulses. For low-noise pulses it is better to operate the laser at moderate power level. However, higher laser power is required for most of the applications. Thus, the noise added during amplification is very important for the noise performance of the ultimate laser signal. A high power fiber laser setup is constructed and the noise performance is characterized with respect to the amplification factor. The system produces sub-160 fs pulses with 10.6 W average power at 43 MHz repetition rate. It is the first amplifier system that is seeded by all-normal dispersion type laser and operates with noise performance better than the solid-state laser systems and comparable to low-noise continuous-wave fiber laser systems. The experience gained from the laser noise research is used to increase the noise performance of the seed laser and the noise added during amplification is analyzed. To the best of our knowledge, it is the first study of the characterization of the intensity noise of fiber amplifiers. The system works in its maximum power with a noise performance better than 0.2% where the seed signals intensity noise is less than 0.03%. The noise increases significantly while increasing the output power of the system, especially in low frequency components. However, comparing with laser operation in high-noise state (the noise level is higher than 1%), using a chain of amplifiers is still the best way to achieve high laser power. To understand what causes the increase in the low frequency noise, modulation transfer function approach is applied.

A modulation transfer function (MTF) defines how the modulations on the pump or seed signal transfer as a modulation on the laser or amplified signals as a function of the modulation frequency. The modulation transfer functions of both Yb-doped fiber laser (YDFL) and Er-doped fiber laser (EDFL) are reported. The MTFs are essentially flat up to a 3 dB cut-off frequency of around 80 kHz for the YDFL and around 15 kHz for the EDFL. The functions are used to predict the laser noise from the noise of pump source, and the prediction supplies a lower limit for the intensity noise of mode-locked laser. It is observed that low frequency components of laser noise are mostly coupled from the pump source. The MTFs are also characterized with respect to the cavity losses, and it is observed that the noise coupled from the pump source increases with cavity losses. The cut-off frequencies also designate the modulation bandwidth of the fiber lasers by using the pump sources. The modulation transfer functions of Yb-doped fiber amplifier from both seed source and pump source are reported. The MTF from the pump source behaves similar to the MTF of YDFL except for the 3-dB cut-off frequency. The cut-off frequency is slightly different due to the oscillatory nature of the laser dynamics. On the other hand, MTF from seed source has opposite manner. The lower frequency components of modulations on the seed signal are suppressed by the gain medium. Hence, the lower frequency components of noise of amplified signal are mostly coupled from pump source, and the higher frequency components are coupled from the seed source. The predicted noise trace supplies a lower limit for the spectral noise density of the ultimate signal. It is also concluded that the pump source (for low frequencies) and seed source (for high frequencies) can be used together for broadband modulation of laser signals.

As a summary, to build an ultra-low noise fiber laser system: (1) the cavity finesse of the seed laser should be as high as possible, (2) the seed laser should operate at moderate power level, (3) use of a chain of amplifiers is advised for avoiding high amplification in a single stage amplifier, and (4) using low noise pump sources is essential. The noise performance of high power fiber laser systems is limited by the noise of pump sources, and will improve with advance in pump laser technology. It is possible to estimate a lower limit for the noise of the ultimate signal by using modulation transfer functions and spectral noise density of pump sources.

Intensity noise determines the minimum detectable level of most of the scientific measurements. As an example, absorption spectroscopy is one of the fundamental techniques to determine the presence of a particular substance or to quantify the amount of substance present in a sample. Since the absorbance is usually small, ultra-low noise laser signals are required to detect such low differences. In this context an ultra-low noise fiber laser setup has been constructed for absorption spectroscopy studies of reactive species in a micro-plasma discharge. This study has been initiated as a scientific collaboration with the plasma research group at Ruhr-University Bochum. The system produces broadband pulses (700 nm at 30 dB bandwidth) with an integrated noise level around 10^{-3}. Consequently, the absorption spectroscopy at around 800 nm for Argon and around 1080 nm for helium species is measured with the sensitivity of 10^{-3}. More sensitive measurement is possible by increasing the measurement time of the experiment. The laser system also produces high-energy pulses, which are able to trigger the ignition of and transition into other transient states of plasma. Since both pulses are generated from the same mode-locked master oscillator, they have excellent synchronization. Thus, we have demonstrated the possibility of pump-probe experiments by initiating breakdown on a picosecond time scale (pump) with a high-power beam and measuring the broadband absorption with the simultaneously provided supercontinuum (probe). The level of synchronization of the two arms is limited by the timing jitter of the mode-locked fiber laser, which is around tens of femtoseconds in free running case.

The stability of the laser is also very important for the technological applications. As an example for ladar application, intensity noise of the transmitter laser affect the range of the measurement and false alert ratio for a fixed measurement time. Furthermore, level of amplified spontaneous emission determines the energy of a single pulse with fixed average power, which also affects the range. Finally, beam quality is essential for transmitting the light with a low divergence angle. Two different fiber laser systems have been constructed as transmitter sources of direct detection and coherent detection ladar systems and are tested for realistic scenarios. Both ladar systems succeeded to detect 1 cm radius wire from 1 km distance with a measurement time shorter than 100 s, which is one of the best performances among the commercial ladar systems. It is concluded that direct detection is more convenient in ranging applications in terms of signal to noise ratio and power requirements. However, coherent detection is also able to provide the velocity information of moving targets, and this capability makes it peerless for specific applications. It can be concluded that a hybrid system can be the best option for ranging and motion detecting. This study concludes that fiber laser systems have tremendous performance as transmitter sources for ladars. The direct detection ladar with the fiber laser system is qualified from the environmental tests. It can operate at the temperatures between −20°C and 50°C and can be stored at the temperatures between −30°C and 60°C. Furthermore, it can survive in the vibration of a Sikorsky helicopter without any change in the performance.

As a summary, fiber laser systems show the tremendous performance for the scientific and technological applications in terms of noise performance and beam quality. Due to their advantage of being compact, alignment-free and robust, they are convenient for being used inside a commercial technological device or as a scientific measurement setup. Modulating the pump power with a feedback signal and carefully isolating the system from environmental noise sources can further decrease the intensity noise of the fiber laser system. Today the intensity noise of fiber laser systems is limited by the noise level of pump sources, and is expected to improve with the development of pump laser technology.

In this century, optics-based technologies are expected to become much more widespread, become an alternative to radio-frequency-based technologies in most of the applications, and pave the way for new application fields. The studies reported in this thesis show the way to build low-noise and long-term-stable fiber laser systems to be used in scientific and technological applications, some of which are listed below as future plans:

- Multidimensional remote sensing devices: Ladar systems, which provide 3 dimensional shapes, vibrational profiles and instantaneous velocities of the targets simultaneously, can be built by using fiber laser systems. Using both the direct detection and coherent detection techniques in a single ladar system will make possible to provide more information from a target for specific applications.

- Fiber-optic acoustic sensors: Fiber laser systems are also suitable for high-performance acoustic sensing applications. Especially for underwater applications, this is a very challenging field in which extreme sensitivity is required to meet very low threshold detection levels in the presence of a very large hydrostatic pressure. This huge dynamic range requirement makes impossible to use most of the linear acoustic sensors. One of the solutions is to interrogate the fiber-optic sensor using interferometric techniques, which simultaneously provides a high sensitivity and a high dynamic range. Our plan is to construct a series of fiber-optic acoustic sensors to detect underwater acoustic signals and determine the direction of the source.

- Three dimensional (3D) scanners and printers: A 3D scanner is an instrument that collects data from a real-world object in its shape and possibly its appearance. Depending on the target geometry, resolution requirement can be a few micrometers. It is possible to achieve sub-micrometer level in range resolution and a few micrometer levels in lateral resolution by using a single-mode fiber laser system as a transmitter source in a coherent detection ranging system. Collected 3D data can be used to reproduce the object with a 3D printer. A 3D printer is a device that is capable of building a 3D solid object from its 3D data. Laser sintering is one of the most common methods, which is being used for printing. To achieve high resolution in material processing with lasers, low noise operation and high beam quality are the most critical requirements. It is possible to achieve micrometer level resolution with a low-noise and single-mode fiber laser system. Building a complete all-optical 3D scanner-printer system, which is capable of producing 3D data of a real-world object, and building a solid object from its 3D data, is our ultimate goal for the future.

Bibliography

[1] G. Agrawal, *Nonlinear Fiber Optics.* Electronics & Electrical, Academic Press, 2007.

[2] A. C. van Heel, “A new method of transporting optical images without aberrations,” 1954.

[3] H. H. Hopkins and N. S. Kapany, “A flexible fibrescope, using static scanning,” 1954.

[4] D. Marcuse, *Light transmission optics.* Van Nostrand Reinhold New York, 1972.

[5] H. Haus, “Mode-locking of lasers,” *Selected Topics in Quantum Electronics, IEEE Journal of*, vol. 6, no. 6, pp. 1173–1185, 2000.

[6] H. A. Haus, “Theory of mode locking with a fast saturable absorber,” *Journal of Applied Physics*, vol. 46, no. 7, pp. 3049–3058, 1975.

[7] M. Hofer, M. E. Fermann, F. Haberl, M. H. Ober, and A. J. Schmidt, “Mode locking with cross-phase and self-phase modulation,” *Opt. Lett.*, vol. 16, pp. 502–504, Apr 1991.

[8] I. Duling III, “Subpicosecond all-fibre erbium laser,” *Electronics Letters*, vol. 27, no. 6, pp. 544–545, 1991.

[9] K. Tamura, C. Doerr, H. Haus, and E. Ippen, “Soliton fiber ring laser stabilization and tuning with a broad intracavity filter,” *Photonics Technology Letters, IEEE*, vol. 6, no. 6, pp. 697–699, 1994.

[10] F. Ilday, J. Buckley, W. Clark, and F. Wise, "Self-similar evolution of parabolic pulses in a laser," *Physical review letters*, vol. 92, no. 21, p. 213902, 2004.

[11] J. Buckley, F. Wise, F. Ilday, and T. Sosnowski, "Femtosecond fiber lasers with pulse energies above 10 nj," *Optics letters*, vol. 30, no. 14, pp. 1888–1890, 2005.

[12] K. Tamura, E. Ippen, H. Haus, and L. Nelson, "77-fs pulse generation from a stretched-pulse mode-locked all-fiber ring laser," *Optics letters*, vol. 18, no. 13, pp. 1080–1082, 1993.

[13] A. Chong, J. Buckley, W. Renninger, and F. Wise, "All-normal-dispersion femtosecond fiber laser," *Opt. Express*, vol. 14, no. 21, pp. 10095–10100, 2006.

[14] C. Bulent Oktem *et al.*, "Soliton–similariton fibre laser," *Nature Photonics*, vol. 4, no. 5, pp. 307–311, 2010.

[15] K. Kieu, W. Renninger, A. Chong, and F. Wise, "Sub-100 fs pulses at watt-level powers from a dissipative-soliton fiber laser," *Optics letters*, vol. 34, no. 5, pp. 593–595, 2009.

[16] H. A. Haus, J. G. Fujimoto, and E. P. Ippen, "Analytic theory of additive pulse and kerr lens mode locking," *Quantum Electronics, IEEE Journal of*, vol. 28, no. 10, pp. 2086–2096, 1992.

[17] K.-H. Hong, A. Siddiqui, J. Moses, J. Gopinath, J. Hybl, F. Ö. Ilday, T. Y. Fan, and F. X. Kärtner, "Generation of 287 w, 5.5 ps pulses at 78 mhz repetition rate from a cryogenically cooled yb: Yag amplifier seeded by a fiber chirped-pulse amplification system," *Optics letters*, vol. 33, no. 21, pp. 2473–2475, 2008.

[18] S. Namiki and H. A. Haus, "Noise of the stretched pulse fiber laser. i. theory," *Quantum Electronics, IEEE Journal of*, vol. 33, no. 5, pp. 649–659, 1997.

[19] R. Paschotta, "Noise of mode-locked lasers (part i): numerical model," *Applied Physics B*, vol. 79, no. 2, pp. 153–162, 2004.

[20] C. Yu, S. Namiki, and H. A. Haus, "Noise of the stretched pulse fiber laser. ii. experiments," *Quantum Electronics, IEEE Journal of*, vol. 33, no. 5, pp. 660–668, 1997.

[21] J. Chen, J. W. Sickler, E. P. Ippen, and F. X. Kärtner, "High repetition rate, low jitter, low intensity noise, fundamentally mode-locked 167 fs soliton er-fiber laser," *Optics letters*, vol. 32, no. 11, pp. 1566–1568, 2007.

[22] H. Byun, D. Pudo, J. Chen, E. P. Ippen, and F. X. Kärtner, "High-repetition-rate, 491 mhz, femtosecond fiber laser with low timing jitter," *Optics letters*, vol. 33, no. 19, pp. 2221–2223, 2008.

[23] P. K. Mukhopadhyay, K. Ozgoren, I. L. Budunoglu, and O. Ilday, "All-fiber low-noise high-power femtosecond yb-fiber amplifier system seeded by an all-normal dispersion fiber oscillator," *Selected Topics in Quantum Electronics, IEEE Journal of*, vol. 15, no. 1, pp. 145–152, 2009.

[24] A. Liem, J. Limpert, H. Zellmer, and A. Tünnermann, "100-w single-frequency master-oscillator fiber power amplifier," *Optics Letters*, vol. 28, no. 17, pp. 1537–1539, 2003.

[25] I. L. Budunoğlu, C. Ülgüdür, B. Oktem, and F. Ö. Ilday, "Intensity noise of mode-locked fiber lasers," *Optics letters*, vol. 34, no. 16, pp. 2516–2518, 2009.

[26] R. P. Scott, C. Langrock, and B. H. Kolner, "High-dynamic-range laser amplitude and phase noise measurement techniques," *Selected Topics in Quantum Electronics, IEEE Journal of*, vol. 7, no. 4, pp. 641–655, 2001.

[27] S. Sanders, N. Park, J. W. Dawson, and K. J. Vahala, "Reduction of the intensity noise from an erbium-doped fiber laser to the standard quantum limit by intracavity spectral filtering," *Applied physics letters*, vol. 61, no. 16, pp. 1889–1891, 1992.

[28] N. R. Newbury and W. C. Swann, "Low-noise fiber-laser frequency combs," *JOSA B*, vol. 24, no. 8, pp. 1756–1770, 2007.

[29] S. Strogatz, *Nonlinear dynamics and chaos: with applications to physics, biology, chemistry and engineering.* Perseus Books Group, 2001.

[30] C. J. Koester and E. Snitzer, "Amplification in a fiber laser," *Applied Optics*, vol. 3, no. 10, pp. 1182–1186, 1964.

[31] D. Strickland and G. Mourou, "Compression of amplified chirped optical pulses," *Optics Communications*, vol. 55, no. 6, pp. 447–449, 1985.

[32] M. Tröbs, C. Fallnich, *et al.*, "Power-and frequency-noise characteristics of an yb-doped fiber amplifier and actuators for stabilization," *Optics express*, vol. 13, no. 6, pp. 2224–2235, 2005.

[33] T. D. Mulder, R. P. Scott, and B. H. Kolner, "Amplitude and envelope phase noise of a modelocked laser predicted from its noise transfer function and the pump noise power spectrum," *Opt. Express*, vol. 16, no. 18, pp. 14186–14191, 2008.

[34] I. L. Budunoglu, K. Gürel, and F. Ö. Ilday, "Characterization of coupling of pump fluctuations to laser in mode-locked yb-doped and er-doped fiber oscillators," in *Conference on Lasers and Electro-Optics*, Optical Society of America, 2010.

[35] B. Niermann, I. Budunoğlu, K. Gürel, M. Böke, F. Ö. Ilday, and J. Winter, "Application of a mode-locked fiber laser for highly time resolved broadband absorption spectroscopy and laser-assisted breakdown on micro-plasmas," *Journal of Physics D: Applied Physics*, vol. 45, no. 24, p. 245202, 2012.

[36] A. Schutze, J. Y. Jeong, S. E. Babayan, J. Park, G. S. Selwyn, and R. F. Hicks, "The atmospheric-pressure plasma jet: a review and comparison to other plasma sources," *Plasma Science, IEEE Transactions on*, vol. 26, no. 6, pp. 1685–1694, 1998.

[37] V. Schulz-von der Gathen, V. Buck, T. Gans, N. Knake, K. Niemi, S. Reuter, L. Schaper, and J. Winter, "Optical diagnostics of micro discharge jets," *Contributions to Plasma Physics*, vol. 47, no. 7, pp. 510–519, 2007.

[38] L. Schaper, S. Reuter, J. Waskoenig, K. Niemi, V. S. von der Gathen, and T. Gans, "The dynamics of radio-frequency driven atmospheric pressure plasma jets," *Journal of Physics: Conference Series*, vol. 162, no. 1, p. 012013, 2009.

[39] J. Waskoenig, K. Niemi, N. Knake, L. M. Graham, S. Reuter, V. S. von der Gathen, and T. Gans, "Diagnostic-based modeling on a microscale atmospheric-pressure plasma jet," *Pure and Applied Chemistry*, vol. 82, no. 6, p. 1209, 2010.

[40] N. Knake, S. Reuter, K. Niemi, V. S. von der Gathen, and J. Winter, "Absolute atomic oxygen density distributions in the effluent of a microscale atmospheric pressure plasma jet," *Journal of Physics D: Applied Physics*, vol. 41, no. 19, p. 194006, 2008.

[41] N. Sadeghi, "Practical aspects of molecular spectroscopy in plasmas 6. molecular spectroscopy techniques applied for processing plasma diagnostics," *Journal of Plasma and Fusion Research*, vol. 80, no. 9, pp. 767–776, 2004.

[42] D. S. Baer and R. K. Hanson, "Tunable diode laser absorption diagnostics for atmospheric pressure plasmas," *Journal of Quantitative Spectroscopy and Radiative Transfer*, vol. 47, no. 6, pp. 455 – 475, 1992.

[43] J. Rpcke, L. Mechold, X. Duten, and A. Rousseau, "A time resolved laser study of hydrocarbon chemistry in h 2 -ch 4 surface wave plasmas," *Journal of Physics D: Applied Physics*, vol. 34, no. 15, p. 2336, 2001.

[44] A. Rousseau, E. Teboul, M. J. v d Sande, and J. A. M. v d Mullen, "Spatially resolved gas temperature measurements by rayleigh scattering in a microwave discharge," *Plasma Sources Science and Technology*, vol. 11, no. 1, p. 47, 2002.

[45] G. Berden, R. Peeters, and G. Meijer, "Cavity ring-down spectroscopy: Experimental schemes and applications," *International Reviews in Physical Chemistry*, vol. 19, no. 4, pp. 565–607, 2000.

[46] Wang, C. and Srivastava, N., "Oh number densities and plasma jet behavior in atmospheric microwave plasma jets operating with different plasma gases (ar, ar/n2, and ar/o2)," *Eur. Phys. J. D*, vol. 60, no. 3, pp. 465–477, 2010.

[47] T. Gherman, E. Eslami, D. Romanini, S. Kassi, J.-C. Vial, and N. Sadeghi, "High sensitivity broad-band mode-locked cavity-enhanced absorption spectroscopy: measurement of ar*(3p2) atom and ion densities," *Journal of Physics D: Applied Physics*, vol. 37, no. 17, p. 2408, 2004.

[48] S. G. Belostotskiy, R. Khandelwal, Q. Wang, V. M. Donnelly, D. J. Economou, and N. Sadeghi, "Measurement of electron temperature and density in an argon microdischarge by laser thomson scattering," *Applied Physics Letters*, vol. 92, no. 22, pp. –, 2008.

[49] S. G. Belostotskiy, V. M. Donnelly, D. J. Economou, and N. Sadeghi, "Spatially resolved measurements of argon metastable ($1s_5$) density in a high pressure microdischarge using diode laser absorption spectroscopy," *Plasma Science, IEEE Transactions on*, vol. 37, no. 6, pp. 852–858, 2009.

[50] S. G. Belostotskiy, T. Ouk, V. M. Donnelly, D. J. Economou, and N. Sadeghi, "Gas temperature and electron density profiles in an argon dc microdischarge measured by optical emission spectroscopy," *Journal of Applied Physics*, vol. 107, no. 5, pp. –, 2010.

[51] C. Penache, M. Miclea, A. Bruning-Demian, O. Hohn, S. Schssler, T. Jahnke, K. Niemax, and H. Schmidt-Bcking, "Characterization of a high-pressure microdischarge using diode laser atomic absorption spectroscopy," *Plasma Sources Science and Technology*, vol. 11, no. 4, p. 476, 2002.

[52] M. Miclea, K. Kunze, U. Heitmann, S. Florek, J. Franzke, and K. Niemax, "Diagnostics and application of the microhollow cathode discharge as an analytical plasma," *Journal of Physics D: Applied Physics*, vol. 38, no. 11, p. 1709, 2005.

[53] G. Cunge, D. Vempaire, M. Touzeau, and N. Sadeghi, "Broadband and time-resolved absorption spectroscopy with light emitting diodes: Application to etching plasma monitoring," *Applied Physics Letters*, vol. 91, no. 23, 2007.

[54] M. Kogelschatz, G. Cunge, and N. Sadeghi, “Identification of halogen containing radicals in silicon etching plasmas and density measurement by uv broad band absorption spectroscopy,” *Journal of Physics D: Applied Physics*, vol. 37, no. 14, p. 1954, 2004.

[55] J.-P. Booth, G. Cunge, F. Neuilly, and N. Sadeghi, “Absolute radical densities in etching plasmas determined by broad-band uv absorption spectroscopy,” *Plasma Sources Science and Technology*, vol. 7, no. 3, p. 423, 1998.

[56] J. K. Ranka, R. S. Windeler, and A. J. Stentz, “Visible continuum generation in air-silica microstructure optical fibers with anomalous dispersion at 800 nm,” *Opt. Lett.*, vol. 25, pp. 25–27, Jan 2000.

[57] J. C. Knight, T. A. Birks, P. S. J. Russell, and D. M. Atkin, “All-silica single-mode optical fiber with photonic crystal cladding,” *Opt. Lett.*, vol. 21, pp. 1547–1549, Oct 1996.

[58] J. Hermann, S. Bruneau, and M. Sentis, “Spectroscopic analysis of femtosecond laser-induced gas breakdown,” *Thin Solid Films*, vol. 453454, no. 0, pp. 377 – 382, 2004. ¡ce:title¿Proceedings of Symposium H on Photonic Processing of Surfaces, Thin Films and Devices, of the E-MRS 2003 Spring Conference¡/ce:title¿.

[59] V. Margetic, A. Pakulev, A. Stockhaus, M. Bolshov, K. Niemax, and R. Hergenrder, “A comparison of nanosecond and femtosecond laser-induced plasma spectroscopy of brass samples,” *Spectrochimica Acta Part B: Atomic Spectroscopy*, vol. 55, no. 11, pp. 1771 – 1785, 2000.

[60] T. Mizunami, N. Kizaki, and K. Nagaiwa, “Microprocessing and microplasma generation by femtosecond laser pulses generated by figure-of-eight erbium-doped fiber-laser amplifier system,” *Japanese Journal of Applied Physics*, vol. 46, no. 8B, pp. 5450–5455, 2007.

[61] D. von der Linde and H. Schüler, “Breakdown threshold and plasma formation in femtosecond laser–solid interaction,” *J. Opt. Soc. Am. B*, vol. 13, pp. 216–222, Jan 1996.

[62] A. Mitchell, G. R. Scheller, R. A. Gottscho, and D. B. Graves, "Photoelectron-initiated avalanches in low-pressure glow discharges," *Phys. Rev. A*, vol. 40, pp. 5199–5207, Nov 1989.

[63] H. Debontride, J. Derouard, P. Edel, R. Romestain, N. Sadeghi, and J. P. Boeuf, "Transient current and sheath motion following the photoelectron-initiated avalanche in dc glow discharges," *Phys. Rev. A*, vol. 40, pp. 5208–5219, Nov 1989.

[64] A. Luque, V. Ratushnaya, and U. Ebert, "Positive and negative streamers in ambient air: modelling evolution and velocities," *Journal of Physics D: Applied Physics*, vol. 41, no. 23, p. 234005, 2008.

[65] J. M. Dudley, G. Genty, and S. Coen, "Supercontinuum generation in photonic crystal fiber," *Rev. Mod. Phys.*, vol. 78, pp. 1135–1184, Oct 2006.

[66] S. Coen, A. H. L. Chau, R. Leonhardt, J. D. Harvey, J. C. Knight, W. J. Wadsworth, and P. S. J. Russell, "Supercontinuum generation by stimulated raman scattering and parametric four-wave mixing in photonic crystal fibers," *J. Opt. Soc. Am. B*, vol. 19, pp. 753–764, Apr 2002.

[67] F. . O. Ilday, H. Lim, J. R. Buckley, and F. W. Wise, "Practical all-fiber source of high-power, 120-fs pulses at 1 μm," *Opt. Lett.*, vol. 28, pp. 1362–1364, Aug 2003.

[68] B. Niermann, M. Bke, N. Sadeghi, and J. Winter, "Space resolved density measurements of argon and helium metastable atoms in radio-frequency generated he-ar micro-plasmas," *The European Physical Journal D*, vol. 60, no. 3, pp. 489–495, 2010.

[69] M. Teobaldelli, A. D. Puig, T. Zenone, M. Matteucci, G. Seufert, and V. Sequeira, "Building a topological and geometrical model of poplar tree using portable on-ground scanning lidar," *Functional Plant Biology*, vol. 35, no. 10, pp. 1080–1090, 2008.

[70] V. Verma, R. Kumar, and S. Hsu, "3d building detection and modeling from aerial lidar data," in *Computer Vision and Pattern Recognition, 2006 IEEE Computer Society Conference on*, vol. 2, pp. 2213–2220, IEEE, 2006.

[71] V. Wulfmeyer and J. Bösenberg, "Ground-based differential absorption lidar for water-vapor profiling: assessment of accuracy, resolution, and meteorological applications," *Applied Optics*, vol. 37, no. 18, pp. 3825–3844, 1998.

[72] K. Browning and R. Wexler, "The determination of kinematic properties of a wind field using doppler radar," *Journal of Applied Meteorology*, vol. 7, no. 1, pp. 105–113, 1968.

[73] J. Skaloud, J. Vallet, K. Keller, G. Veyssiere, and O. Kölbl, "Helimap: Rapid large scale mapping using handheld lidar/ccd/gps/ins sensors on helicopters," in *Proceedings of the 18th International Technical Meeting of the Satellite Division of The Institute of Navigation (ION GNSS 2005)*, pp. 2461–2467, 2001.

[74] K. T. Bates, F. Rarity, P. L. Manning, D. Hodgetts, B. Vila, O. Oms, À. Galobart, and R. L. Gawthorpe, "High-resolution lidar and photogrammetric survey of the fumanya dinosaur tracksites (catalonia): implications for the conservation and interpretation of geological heritage sites," *Journal of the Geological Society*, vol. 165, no. 1, pp. 115–127, 2008.

[75] L. D. Smullin and G. Fiocco, "Optical echoes from the moon," *Nature*, 1962.

[76] G. Fiocco and L. Smullin, "Detection of scattering layers in the upper atmosphere (60-140 km) by optical radar," *Nature*, vol. 199, pp. 1275–1276, 1963.

[77] R. G. Plumb, "Distributed feedback laser," Mar. 14 1989. US Patent 4,813,054.

[78] E. Burrows and K.-Y. Liou, "High resolution laser lidar utilising two-section distributed feedback semiconductor laser as a coherent source," *Electronics Letters*, vol. 26, no. 9, pp. 577–579, 1990.